Evaluation of a Sliding Mode Fault Tolerant Controller for the EL-AL Incident

H. Alwi, C. Edwards, O. Stroosma and J. A. Mulder

Abstract

This paper presents piloted flight simulator results associated with the EL-AL flight 1862 scenario using a model reference–based sliding mode control allocation scheme for fault tolerant control. The proposed controller design was carried out without any knowledge of the type of failure, and in the absence of any fault detection and isolation strategy. This is motivated by the fact that the flight crew were unaware of the loss of the right engines. For this reason, the control allocation scheme which is proposed uses (fixed) equal distribution of the control signals to all actuators (for both nominal situations and when a fault or failure occurs). The paper analyzes the scheme and determines the conditions under which closed-loop stability is retained. The results represent the successful real-time implementation of the proposed controller on the SIMONA motion flight simulator configured to represent a B747 aircraft. The evaluation results from the experienced pilots show that the proposed controller has the ability to position the aircraft for landing in both a nominal and the EL-AL failure scenario. It is also shown that actuator faults and failures which occured during the EL-AL incident can be handled directly without reconfiguring the controller.

NOMENCLATURE

6–DOF	= 6 degree of freedom
EPR	= engine pressure ratio
cmd	= command signal
ru, rl	= upper and lower rudders
sp	= spoiler
air, ail, aor, aol	= inboard right, inboard left, outboard right and outboard left ailerons
p, q, r	= roll, pitch and yaw rate (rad/s)
V_{tas}	= true air speed (m/s)
α, β	= angle of attack and sideslip angle (rad)
ϕ, θ, ψ	= roll, pitch and yaw angle (rad)
h_e, x_e, y_e	= geometric earth position along the z (altitude), x and y axis (m)
$\bar{\lambda}(\cdot), \underline{\lambda}(\cdot)$	= largest and smallest eigenvalues
$\|\cdot\|$	= Euclidean norm (vectors) or induced spectral norm (matrices)
$u(t), \nu(t)$	= actual and virtual control input
$\mathbb{R}$	= field of real numbers and the set of strictly positive real numbers
s, σ	= Laplace variable, Sliding mode switching function
$lat, long$	= lateral and longitudinal axis
FTC, FDI	= Fault Tolerant Control, Fault Detection and Isolation
SMC	= sliding mode control
SRS	= SIMONA research simulator
DME	= distance measurement equipment
ILS	= instrument landing system
APP	= approach (button on the mode control pannel)
LOC, GS	= localizer, glide slope
MCP	= mode control panel
FPA	= flight path angle
FBW	= fly by wire

H. Alwi and C. Edwards are with the College of Engineering, Mathematics and Physical Sciences, University of Exeter, EX4 4QF, UK. h.alwi@exeter.ac.uk, C.Edwards@exeter.ac.uk

O. Stroosma and J. A. Mulder are with the Control and Simulation section of the Faculty of Aerospace Engineering, Delft University of Technology, Kluyverweg 1, 2629HS, The Netherlands. O.Stroosma@tudelft.nl, J.A.Mulder@tudelft.nl

I. INTRODUCTION

Lessons learnt from previous incidents where pilots successfully landed damaged aircraft – such as Flight 232 (DC-10) in Sioux City, Iowa 1989[1], the Kalita Air freighter (B747) in Detroit, Michigan, October 2004[2] and the DHL freighter (A300) incident in Baghdad, November 2003[3] – suggest that in many cases, damaged/faulty aircraft are still 'flyable' and controllable with some level of performance, which makes it possible for the pilot to safely land the aircraft. This has also been shown by a successful program carried out by NASA on propulsion controlled aircraft (as described in the work of Burcham *et al.*[3], [4], [5], Tucker *et al.*[6] and Burken *et al.*[7] – which consider MD-11, B747, C17 and F15 aircraft), which showed that the controllers developed during the study helped the pilots to land the aircraft safely in the event of total hydraulic loss (Tucker [6]). An independent investigation of the EL-AL flight 1862 which crashed into an apartment building in Bijlmermeer, Amsterdam, conducted by Delft University (Smaili & Mulder [8]), suggested that there was still some manoeuvering capability associated with the damaged aircraft. This is backed up by an early publication on Fault Tolerant Control (FTC) by Maciejowski & Jones [9] which showed that it was possible to control the damaged aircraft via a Model Predictive Control (MPC) scheme (although Maciejowski & Jones [9] assume an exact post–damage model is available). Subsequent work by Hennig & Balas [10] on MPC for FTC, also considers the EL-AL 1862 scenario.

The EL-AL flight 1862 scenario was used as the basis for the GARTEUR (Group for Aeronautical Research and Technology in Europe) Flight Mechanics Action Group 16 (FM–AG16) which explored and assessed the use of modern Fault Detection and Isolation (FDI) and FTC strategies to improve flight safety. Recent papers from the GARTEUR FM-AG16 program include Lombaerts *et al.*[11] (which uses adaptive nonlinear dynamic inversion) while the paper by Stroosma *et al.*[12] discusses simulator evaluations of different FM-AG16 controllers.

The work in Shtessel *et al.*[13] and Wells & Hess [14] provides practical examples of the combination of Sliding Mode Control (SMC) and Control Allocation (CA) for FTC. These papers exploit the inherent robustness of sliding modes, which when integrated with control allocation, allow total failures of certain actuators to be accommodated. More recently in Alwi & Edwards [15], [16] a sliding mode control allocation scheme was proposed. Easily testable conditions were developed to guarantee the stability of the closed-loop system subject to a certain class of actuator faults (which will be described precisely later in the paper). The scheme in Alwi & Edwards [16] uses a control law which depends on (an estimation of) the 'efficiency/effectiveness' of the actuators.

This paper presents the SIMONA 6-DOF motion flight simulator results, obtained by airline and test-pilots, with experience covering B747, B767, A330 and Citation II aircraft on the EL-AL flight 1862 (Bijlmermeer incident) scenario – which is one of the case studies associated with the GARTEUR FM–AG16. The results in this paper are the outcome of the controller evaluation flight testing campaign and the GARTEUR FM–AG16 final workshop at Delft University, The Netherlands. The results presented represent the successful real–time implementation of the proposed sliding mode controller on SIMONA.

The controller that has been used is a modification of the model reference sliding mode controller proposed by Alwi & Edwards [15]. The model reference tracking framework chosen in this paper has advantageous features – especially the absence of integrators – when compared with the controller in Alwi *et al.*[17]. The absence of integrators eliminates the dangers of controller windup in the face of saturation and rate limits being exceeded during faults, failures or structural damage. Another advantageous feature of the model reference framework is that the performance specifications are predefined and are represented in terms of an ideal transfer function response.

In this paper, the situation which occurred during the EL-AL flight 1862, whereby the flight crew were unaware that engines no. 3 and 4 had separated from the wing (despite reporting the loss of thrust from both engines), will be assumed. This is the motivation for the tests carried out in this paper which are all performed under the assumption that the type of failure is unknown and in the absence of any FDI or fault reconstruction strategy. Therefore the controller has been designed with no knowledge of the failure and damage to the airframe. Since there is no FDI and no actuator effectiveness estimation available, a fixed control allocation approach (as described in Alwi *et al.*[17]) will be used. The fixed control allocation scheme is sufficient to access the remaining available

[1]Flight 232 suffered tail engine failure that caused the total loss of hydraulics (Burcham *et al.*[1] and Gero [2]).

[2]The freighter shed engine no. 1, but the crew managed to land safely without any casualties.

[3]The DHL A300B4 was hit by a missile on its left wing and lost all hydraulics, but still landed safely(Burcham *et al.*[1]).

control surfaces capability and 'passively'[4] controls the aircraft, exploiting the robustness properties of sliding mode controllers, to ensure stability, and some nominal performance.

The controller has been designed as an 'autopilot' which receives pilot set-points from the mode control panel in order to change roll, sideslip, flight path angle and speed. An outer-loop heading & altitude change/hold and ILS landing approach has also been included to provide assistance to positioned the aircraft for landing.

II. Test facilities (SIMONA)

The FTLAB747 software (representing a high fidelity 6-DOF rigid body aerodynamic model of the B747-100/200 aircraft) which runs on MATLAB,[5] has been developed by several researchers (van der Linden[20], Smaili[21] and Marcos & Balas [22]). The 77 state FTLAB747 model consists of the 12 rigid body states, and incorporates detailed dynamical models of the sensors and actuators – together with realistic position and rate limits. This software has been used as a realistic platform to test FTC and FDI schemes by many researchers e.g. Hennig & Balas [10], Marcos & Balas [23], Marcos *et al.*[24], Szaszi *et al.*[25] and Zhou *et al* [26]. In its latest incarnation, it has been used as part of the GARTEUR FM-AG16 group as a benchmark (and described in detail Smaili *et al.*[27]).

(a) Outside view (b) Flight deck view

Fig. 1. SIMONA research simulator

The SIMONA (SImulation, MOtion and NAvigation) Research Simulator (SRS) shown in Figure 1 is a pilot-in-the-loop flight simulator with motion capabilities operated by Delft University of Technology. It provides researchers with a powerful tool that can be adapted to various uses (Stroosma *et al.*[28]). The simulator's flexible software architecture and high-fidelity cueing environment allows the integration of the aircraft model from Smaili et al. [27]. Its inputs and outputs were standardized to fit the SRS software environment and the SIMULINK model was converted to C code using Real-Time Workshop. Finally the model was integrated with the pilot controls, aircraft instruments (Figure 1(b)) and other cueing devices of the SRS (i.e. outside visual and motion systems). On the flight deck of the SRS, the evaluation pilot was presented with flight instruments representative of a B747 aircraft, a control column with appropriate feel system dynamics, a central pedestal with dual engine controls, a Mode Control Panel (MCP) for controlling the autopilot and a wide collimated view on a virtual outside world. The simulator's motion system was tuned to give the pilot realistic inertial motion cues in nominal and failure conditions.

III. EL-AL flight 1862: the incident

On the 4th October 1992, the EL-AL flight 1862 freighter aircraft – a Boeing 747-200 – (on a scheduled flight from New York JFK airport to Tel Aviv Israel) departed from Schiphol Airport, Amsterdam after refuelling and a crew change. Shortly after takeoff, as the aircraft reached an altitude of about 6500ft, the pilots transmited an emergency call. The crew reported a fire in engine no. 3 and reported the loss of thrust in engines no. 3 and 4 as the aircraft was turning to the right. As described in the incident report by the Netherlands Aviation Safety Board

[4]Here 'passive' refers to 'passive' fault tolerant controllers, which are defined by Patton [18] and Zhang & Jiang [19] as controllers that are robust and insensitive to certain faults without use of on-line fault information and without requiring controller reconfiguration.

[5]MATHWORKS trademark

[29], the pilots were operating under extreme workload conditions trying to control the aircraft. Straight and level flight required full left (positive) rudder pedal deflection and 60% to 70% maximum lateral control (the wheel almost full to the left (negative)) [29]. A series of right hand turns were performed in order to land in runway 27. The first attempt to intercept the localizer and align for the final approach course was unsuccessful as the aircraft overshot the localizer. Shortly after, the crew reported that engines no. 3 and 4 were inoperative and reported a problem on the wing flaps. During the second attempt to intercept the localizer, a heading and altitude change to 310° and 1500ft respectively were requested. The flight crew immediately reported control difficulties. The aircraft crashed 13km east of Schiphol airport into an apartment building in Bijlmermeer, a suburb of Amsterdam. Further details on the incident can be found in the accident report by the Netherlands Aviation Safety Board [29].

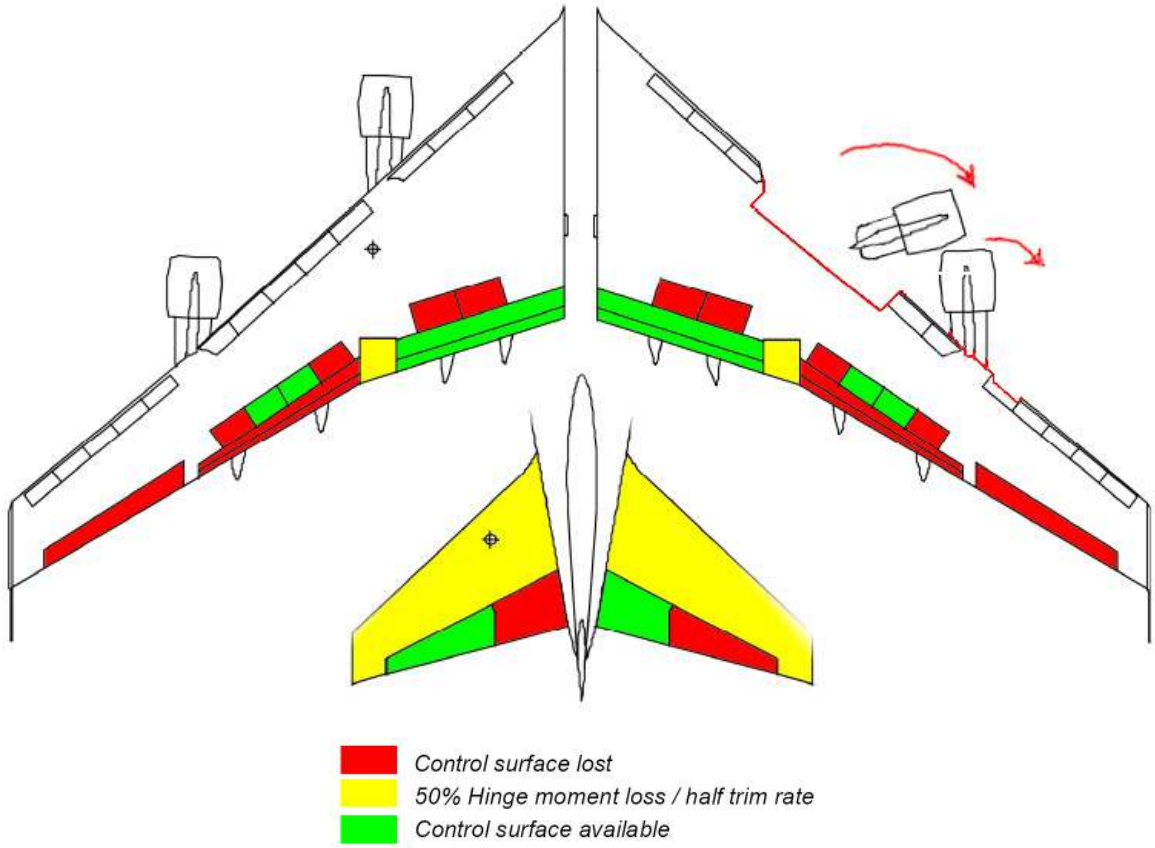

Fig. 2. EL-AL flight 1862: actuator fault/failure and structural damage (adapted from the EL-AL incident report [29] and Smaili *et al.*[27])

It is important to highlight that, for the duration of the incident, the flight crew was unaware that engines no. 3 and 4 had separated from the wing, despite reporting loss of thrust from both engines. Unknown to the flight crew, the inboard fuse-pin[6] that held engine no. 3 to the pylon broke due to fatigue. This caused no. 3 engine and its pylon to separate from the right wing shortly after takeoff causing damage to the leading edge of the right wing. The shedding of engine no. 3 from the right wing in an outboard and rearward direction resulted in a collision with no. 4 engine (see Figure 2), causing it and its pylon to separate from the wing. Figure 2 illustrates the estimated damage thought to have occurred on the right wing. (Smaili *et al.*[27] argue that, although only engine no. 2 was shed in the accident at Anchorage on March 31, 1993, the amount of damage on the wing leading edge, as shown in Figure 3, is probably indicative of the damage inflicted on the El Al 1862 wing).

The damage and the effect on the EL-AL flight 1862 aircraft, as described by Smaili *et al.*[27], are:

1) Aircraft systems
   - loss of hydraulic systems no. 3 and 4;

[6]The role of the fuse pin is to allow the engine to separate from the wing under a strong impact that occurs in the event of a crash or hard landing in order to protect the fuselage from engine fire.

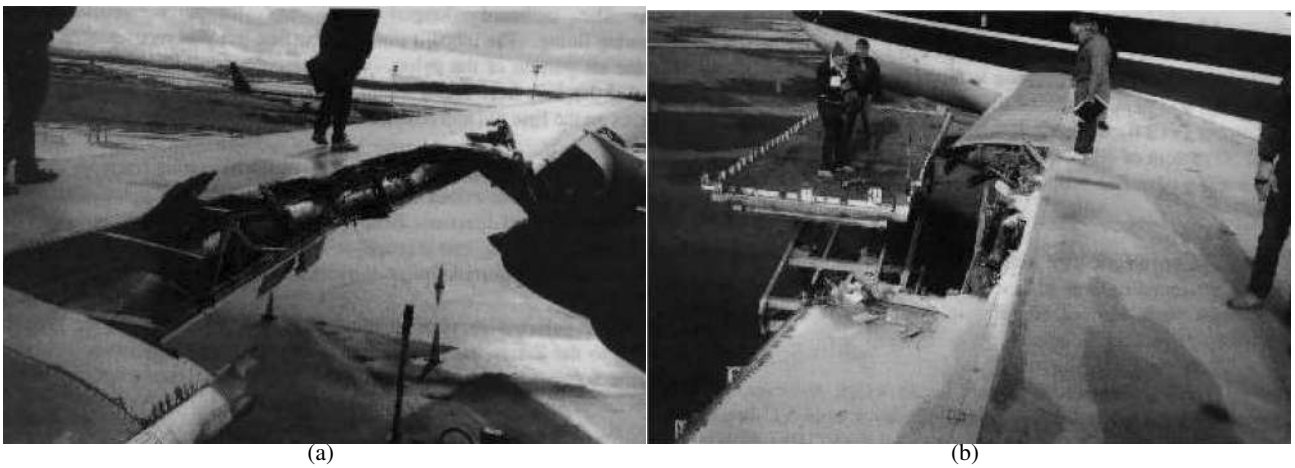

(a) (b)

Fig. 3. Wing damage due to separation of engine no. 2, Anchorage, 1993 (adapted from Smaili *et al.*[27])

- a right (positive) yawing moment due to asymmetric thrust from engines no. 1 and 2;

2) Mass properties
   - a mass reduction of about 10 tonnes resulting from the loss of engines no. 3 and 4 (and the pylons);
   - lateral CG displacement (towards the left wing) due to the loss of the engines;
3) Aerodynamics
   - lift loss on the right wing and additional drag caused by the damaged leading edge;
   - changes to the roll pitch and yaw moment caused by the wing damage;
   - loss of efficiency of the right inboard aileron and spoilers 10 & 11, due to airflow disruption caused by the damaged right wing leading edge.

Figure 2 summarizes the losses and the remaining functional control surfaces (due to the loss of hydraulic systems no. 3 and 4 as described in the incident report [29]). The control surfaces lost due to the failure of hydraulic systems no. 3 and 4 are the outboard trailing edge flaps, the right outboard aileron, spoilers 1,4,5,8,9 & 12, the left inboard elevator and the right outboard elevator. The control surfaces which are still functional but are affected by the loss of the hydraulic systems, are the horizontal stabilizer, the inboard ailerons (both at half rate) and the lower rudder (lag). Although the right inboard aileron and spoilers 10 and 11 remain fully functional, the airflow disruption, resulting from the damage to the leading edge of the right wing, reduces their aerodynamic efficiency and their capacity to provide a roll moment. The only fully functional control surfaces are the inboard trailing edge flaps, spoilers 2 & 3, the left outboard elevator and the right inboard elevator.

Early FTC studies on the EL-AL flight 1862 by Maciejowski & Jones [9] showed that it is possible to control the damaged aircraft (although Maciejowski & Jones [9] assumed an accurate model of the damaged aircraft was available to the controller – either from an FDI scheme or from system identification/estimation).

IV. A MODEL REFERENCE SLIDING MODE CONTROL ALLOCATION SCHEME

This paper considers a situation where a fault associated with the actuators develops in a system. It will be assumed that the system subject to actuator faults or failures, can be written as

$$\dot{x}(t) = (A + A^{\delta}(t))x(t) + Bu(t) - BK(t)u(t) + BK(t)d(t) \tag{1}$$

where $A \in \mathbb{R}^{n_x \times n_x}$ and $B \in \mathbb{R}^{n_x \times n_u}$. Structural damage is described by a change in the system matrix A represented by $A^{\delta}(t)$. The effectiveness gain $K(t) := \text{diag}(k_1(t), \ldots, k_{n_u}(t))$, where the $k_i(t)$ are scalars satisfying $0 \leq k_i(t) \leq 1$. These scalars model a decrease in effectiveness of a particular actuator. If $k_i(t) = 0$, the ith actuator is working perfectly whereas if $k_i(t) > 0$, a fault is present, and if $k_i(t) = 1$ the actuator has failed completely. The exogenous signal $d(t)$ represents a disturbance which may impact on the system as a result of a fault/failure: for example, the moment generated by a control surface which has stuck in a non-neutral position in control channel i could be modelled as $k_i = 1$ and $d_i \neq 0$.

Remark: The control law based on the model in (1) i.e. from a linearization about an operating condition is likely only to be applicable over part of the flight envelope, and will rely on the robustness properties of the controller.

In most control allocation (CA) strategies, the control signal is distributed equally among all the actuators (Shin *et al.*[30], Shtessel *et al.*[13] and Wells & Hess [14]) or distributed based on the limits (position and rate) of the actuators (Härkegård & Glad [31]). In papers by Alwi & Edwards [15], [16], information about $K(t)$ has been incorporated into the allocation algorithm through a weighting matrix W, so that the control is redistributed to the remaining healthy actuators when faults/failures occur. In this paper, the CA strategy is based on the widely used approaches from the literature; i.e. fixed and equal distribution of the control signals. This is motivated by the fact that the information about $K(t)$ in (1) is not always available and mirrors what happened during the EL-AL flight 1862 scenario.

The input distribution matrix B from (1) is assumed to have been reordered and partitioned as:

$$B = \begin{bmatrix} B_1 \\ B_2 \end{bmatrix} \tag{2}$$

where $B_1 \in \mathbb{R}^{(n_u - n_\nu)\times n_u}$ and $B_2 \in \mathbb{R}^{n_\nu \times n_u}$ has rank $n_\nu < n_u$. The partition is in keeping with the notion of splitting the control law from the control allocation task (Härkegård & Glad [32] and Beck [33]). In aircraft systems, the overall control objectives can be successfully achieved by generating appropriate moments about the principal axes by use of the control surfaces (Härkegård & Glad [32] and Beck [33]). In this paper, B_2 is associated with the equations of angular acceleration in roll, pitch and yaw [31], although in principle, this can be extended to other systems which may have no partition of the control law (Beck [33]). In this paper, the matrix B_2 represents the dominant contribution of the control action on the system, while B_1 generally will have elements of small magnitude compared with $\|B_2\|$. This formulation is more general when compared earlier work – for example by Shin *et al.*[30] where it is assumed that $B_1 = 0$. It will be assumed without loss of generality that the states of the system in (1) have been transformed so that $B_2 B_2^{\mathrm{T}} = I_{n_\nu}$ and therefore $\|B_2\| = 1$. Let the 'virtual control'[7] be given by

$$\nu(t) := B_2 u(t) \tag{3}$$

so that

$$u(t) = B_2^{\dagger} \nu(t) \tag{4}$$

where the right pseudo inverse[8] is chosen as

$$B_2^{\dagger} := B_2^{\mathrm{T}} \tag{5}$$

The pseudo-inverse in (5) arises from the optimization problem

$$\min_u \|u\|^2 \quad \text{subject to } B_2 u = \nu \tag{6}$$

Remark: Note that, compared with (6), there exist more general optimization problem formulations for control allocation (see for example Enns [36] and Durham[37]). However, in the context of this paper, especially for the real-time SIMONA implementation, it will be shown that one of the key issues is the onboard computational constraint. By adopting a simple optimization approach as in (6), the real-time computational constraints can be met, thus allowing successful real time implementation.

In the event of faults/failures or structural damage to the aircraft, equilibrium needs to be achieved first. The damage on the wing in the EL-AL incident caused a nonzero roll, pitch and yaw moment. Therefore in order to achieve equilibrium, control surface trims are required. During the actual incident, the pilots managed to achieve an equilibrium condition of straight and level flight by manipulating the control surfaces. In this paper, the changes in the trim condition will be automatically compensated for by the controller, and no pilot input is required. In terms of the stability analysis which follows, the effect of the exogenous disturbance $d(t)$ from (1) is ignored. Clearly

[7]In this context, virtual control refers to a fictitious 'control input' which is used for control law design, and not the actual plant inputs. The mapping between the virtual inputs and the true inputs is the problem of control allocation (Härkegård [32]).

[8]In linear algebra terms, a pseudo inverse is a generalization of the inverse matrix (Horn & Johnson [34] and Penrose [35]). For a non square matrix, a perfect inverse is not available, and therefore an approximate inverse i.e. a pseudo inverse is used. Here $B_2^{\dagger}$ has the property that $B_2 B_2^{\dagger} = I_{n_\nu}$ whilst solving the optimization problem in (6).

this external signal does not formally affect the stability or otherwise of the closed-loop system associated with (1) – although of course it affects the closed-loop performance of the system. In the real system, it will directly affect the trim points and flight envelope of the damaged aircraft. In the following stability analysis $d \equiv 0$. The development which follows is similar in spirit to Alwi & Edwards [16] but is different in detail because of the model reference setting. Using (4) and (5), it can be shown that (1) can be written as

$$\dot{x}(t) = (A + A^{\delta}(t))x(t) + \underbrace{\begin{bmatrix} B_1 B_2^{\mathrm{T}} \\ I \end{bmatrix}}_{B_\nu} \nu(t) - \underbrace{\begin{bmatrix} B_1 K B_2^{\mathrm{T}} \\ B_2 K B_2^{\mathrm{T}} \end{bmatrix}}_{\bar{B}_k} \nu(t) \tag{7}$$

In the nominal fault–free case $A^{\delta}(t) = 0$, $K = 0$ and $\bar{B}_k$ in (7) is zero. Consider a reference model defined as

$$\dot{x}_m(t) = A_m x_m(t) + B_m y_d(t) \tag{8}$$

where $y_d(t)$ is the reference signal and $A_m \in \mathbb{R}^{n_x \times n_x}$, $B_m \in \mathbb{R}^{n_x \times n_\nu}$ with A_m stable. Define

$$e(t) = x(t) - x_m(t) \tag{9}$$

and therefore from (7) and (8) the error system

$$\dot{e}(t) = (A + A^{\delta}(t))e(t) + (A^{\delta}(t) + A - A_m)x_m(t) + B_\nu \nu(t) - \bar{B}_k \nu(t) - B_m y_d(t) \tag{10}$$

The matrices A_m and B_m in (8) represent the reference model which defines the required closed-loop system performance. Here the reference model matrices A_m and B_m are chosen as

$$A_m = A + B_\nu F, \quad B_m = B_\nu G \tag{11}$$

Other approaches to define the ideal model can be adopted (see for example Landau *et al.*[38], [39] and Monopoli & Subbarao [40]), but here the formulation which has been traditionally incorporated within a sliding mode framework has been employed (Broussard & O'Brien [41], and Zinober *et al.*[42]). The matrices F and G represent the feedback and feed–forward terms which define the reference model. Based on these matrices, define a feed-forward signal as

$$\nu_m(t) := F x_m(t) + G y_d(t) \tag{12}$$

Sliding mode techniques (Utkin[43] and Edwards & Spurgeon [44]), will now be used to synthesize $\nu(t)$. The control objective seeks to minimize the error between the reference model and the 'virtual' controlled plant (A, B_ν) in (7). Define a so–called switching function $\sigma : \mathbb{R}^{n_x} \to \mathbb{R}^{n_\nu}$ to be

$$\sigma(t) = Se(t) \tag{13}$$

where the design parameter $S \in \mathbb{R}^{n_\nu \times n_x}$ and $\det(SB_\nu) \neq 0$ by construction. Let $\mathcal{S}$ be the hyperplane defined by $\mathcal{S} = \{e(t) \in \mathbb{R}^{n_x} \ : \ Se(t) = 0\}$. If a control law can be developed which forces the closed-loop trajectories onto the surface $\mathcal{S}$ in finite time and constrains the states to remain there, then an ideal sliding motion is said to have been attained (Edwards & Spurgeon [44]). The sliding surface will be designed based on the nominal no fault condition ($K = 0$). Using (11), equation (10) can be rewritten as

$$\dot{e}(t) = (A + A^{\delta}(t))e(t) + A^{\delta}(t)x_m(t) - \bar{B}_k \nu(t) + B_\nu(\nu(t) \underbrace{- F x_m(t) - G y_d(t)}_{-\nu_m(t)}) \tag{14}$$

where B_ν and $\bar{B}_k$ are defined in (7). A coordinate transformation $e \mapsto T_r e(t) = \hat{e}(t)$ is introduced to obtain 'regular form' (Utkin [43] and Edwards & Spurgeon [44]). If

$$T_r := \begin{bmatrix} I & -B_1 B_2^T \\ 0 & I \end{bmatrix} \tag{15}$$

then using similar argument to those in Alwi & Edwards [45], equation (14) becomes:

$$\dot{\hat{e}}(t) \ = \ (\hat{A} + \hat{A}^{\delta})\hat{e}(t) + \hat{A}^{\delta}\hat{x}_m(t) + \underbrace{\begin{bmatrix} 0 \\ I \end{bmatrix}}_{\hat{B}_\nu} (\nu(t) - \nu_m(t)) - \begin{bmatrix} -B_1 B_2^N (I - K) B_2^{\mathrm{T}} \\ I - B_2 (I - K) B_2^{\mathrm{T}} \end{bmatrix} \nu(t) \tag{16}$$

where $\hat{A} := T_r A T_r^{-1}$, $\hat{A}^\delta := T_r A^\delta T_r^{-1}$ and $\hat{x}_m = T_r x_m(t)$. The projection operator is

$$B_2^N := (I - B_2^{\mathrm{T}} B_2) \tag{17}$$

Because by construction the matrix $B_2 B_2^{\mathrm{T}} = I_l$, it follows that $B_2^N B_2^{\mathrm{T}} = (I - B_2^{\mathrm{T}} B_2) B_2^{\mathrm{T}} = 0$. Therefore, the last term in (16) is zero in a fault–free case ($K = 0$), but is treated as (unmatched) uncertainty when $K \neq 0$. Define

$$W := I - K \tag{18}$$

and write

$$B_2^+ := W B_2^{\mathrm{T}} (B_2 W B_2^{\mathrm{T}})^{-1} \tag{19}$$

As shown in Stewart [46], there exists a scalar γ_0 which is finite and independent of W such that

$$\| B_2^+ \| = \| W B_2^{\mathrm{T}} (B_2 W B_2^{\mathrm{T}})^{-1} \| < \gamma_0 \tag{20}$$

for all $W = diag(w_1 \dots w_{n_u})$ such that $0 < w_i \leq 1$.

The development now diverges from the exposition in Alwi & Edwards [16] because of the inclusion of the parametric uncertainty not analyzed in Alwi & Edwards [16]. A virtual control law will now be designed based on the nominal fault-free system in which the last term in (16) is zero. In the $\hat{e}(t)$ coordinates, a suitable choice for the sliding surface matrix is

$$\hat{S} = S T_r^{-1} = \left[\begin{array}{cc} M & I \end{array} \right] \tag{21}$$

where $M \in \mathbb{R}^{n_\nu \times (n_x - n_\nu)}$ represents design freedom. Introduce another transformation $(\hat{e}_1, \hat{e}_2) \mapsto (\hat{e}_1, \sigma) = \tilde{e}$, associated with

$$T_\sigma = \left[\begin{array}{cc} I & 0 \\ M & I \end{array} \right] \tag{22}$$

Equation (16) then becomes

$$\begin{aligned} \left[\begin{array}{c} \dot{\hat{e}}_1(t) \\ \dot{\sigma}(t) \end{array} \right] &= \left[\begin{array}{cc} \tilde{A}_{11} + \tilde{A}_{11}^\delta & \tilde{A}_{12} + \tilde{A}_{12}^\delta \\ \tilde{A}_{21} + \tilde{A}_{21}^\delta & \tilde{A}_{22} + \tilde{A}_{22}^\delta \end{array} \right] \left[\begin{array}{c} \hat{e}_1(t) \\ \sigma(t) \end{array} \right] + \left[\begin{array}{c} \tilde{A}_1^\delta \\ \tilde{A}_2^\delta \end{array} \right] \tilde{x}_m(t) \\ &+ \left[\begin{array}{c} 0 \\ I \end{array} \right] (\nu(t) - \nu_m(t)) - \left[\begin{array}{c} -B_1 B_2^N W B_2^{\mathrm{T}} \\ I - M B_1 B_2^N W B_2^{\mathrm{T}} - B_2 W B_2^{\mathrm{T}} \end{array} \right] \nu(t) \end{aligned} \tag{23}$$

In the above equation, $\tilde{A}_{11} := \hat{A}_{11} - \hat{A}_{12} M$, $\tilde{A}_{21} := M \tilde{A}_{11} + \hat{A}_{21} - \hat{A}_{22} M$, where

$$\hat{A} = \left[\begin{array}{cc} \hat{A}_{11} & \hat{A}_{12} \\ \hat{A}_{21} & \hat{A}_{22} \end{array} \right] \quad \text{and} \quad \tilde{A}^\delta = \left[\begin{array}{cc} \tilde{A}_{11}^\delta & \tilde{A}_{12}^\delta \\ \hline \tilde{A}_{21}^\delta & \tilde{A}_{22}^\delta \end{array} \right] = \left[\begin{array}{c} \tilde{A}_1^\delta \\ \hline \tilde{A}_2^\delta \end{array} \right] \tag{24}$$

and $\mathrm{col}(\tilde{x}_{m_1}, \tilde{x}_{m_2}) = \tilde{x}_m = T_\sigma \hat{x}_m$.

If a control law can be designed to induce a sliding motion, then during sliding, $\dot{\sigma}(t) = \sigma(t) = 0$ and the equivalent control necessary to maintain sliding is obtained from solving for $\nu_{eq}(t)$ from the lower equations of (23) to give

$$\nu_{eq}(t) = (B_2 W B_2^{\mathrm{T}})^{-1} (I + M B_1 B_2^N B_2^+)^{-1} (- (\tilde{A}_{21} + \tilde{A}_{21}^\delta) \hat{e}_1(t) + \nu_m(t) - \tilde{A}_2^\delta \tilde{x}_m(t)) \tag{25}$$

where B_2^N and B_2^+ are defined in (17) and (19) respectively. Assume the sliding surface matrix M has been designed, so that $\tilde{A}_{11} := \hat{A}_{11} - \hat{A}_{12} M$ is stable and $\| M B_1 B_2^N B_2^+ \| < 1$ for all $0 < W \leq I$.

Remark: $\| M B_1 B_2^N B_2^+ \| < 1$ guarantees the inverse in (25) exists and uses the boundedness result from (20). If the inverse in (25) cannot be guaranteed to exist, the sliding motion cannot be guaranteed. Inequality $\| M B_1 B_2^N B_2^+ \| < 1$ depends on both the hyperplane design (through M) and the faults/failures – since B_2^+ depends directly on W.

If (A, B_ν) is controllable, then $(\hat{A}_{11}, \hat{A}_{12})$ from (24) is controllable (Edwards & Spurgeon [44]) and so M can be chosen to make $\hat{A}_{11} - \hat{A}_{12} M$ stable. Substituting (25) into the top partition of (23), yields the following reduced order system which governs the sliding motion:

$$\begin{aligned} \dot{\hat{e}}_1(t) = ((\tilde{A}_{11} + \tilde{A}_{11}^\delta) - B_1 B_2^N B_2^+ (I + M B_1 B_2^N B_2^+)^{-1} (\tilde{A}_{21} + \tilde{A}_{21}^\delta)) \hat{e}_1(t) \\ + B_1 B_2^N B_2^+ (I + M B_1 B_2^N B_2^+)^{-1} (\nu_m(t) - \tilde{A}_2^\delta \tilde{x}_m(t)) \end{aligned} \tag{26}$$

In the event of faults/failures, stability of the system in (26) (which depends on W through B_2^+) needs to be established.

A. Stability analysis

The stability of the sliding mode is dependent on the reduced order system (26). Since by construction, the reference model is stable, for a bounded signal $y_d(t)$, the signal $x_m(t)$ is bounded and hence ν_m from (12) is bounded. Therefore the stability of the reduced order system which governs the sliding motion depends on:

$$\dot{\hat{e}}_1(t) = ((\tilde{A}_{11} + \tilde{A}^{\delta}_{11}) - B_1 B_2^N B_2^+ (I + M B_1 B_2^N B_2^+)^{-1}(\tilde{A}_{21} + \tilde{A}^{\delta}_{21}))\hat{e}_1(t) \tag{27}$$

In a fault–free case, $W = I$, $\tilde{A}^{\delta}_{11} = \tilde{A}^{\delta}_{21} = 0$, and the system in (27) 'collapses' to $\dot{\hat{e}}_1(t) = \tilde{A}_{11}\hat{e}_1(t)$ which is the nominal sliding mode reduced order system for which M has been designed to guarantee stability. In the case when actuator faults/failure occurs but there is no structural damage, $\tilde{A}^{\delta} = 0 \Rightarrow \tilde{A}^{\delta}_{11} = \tilde{A}^{\delta}_{21} = 0$ and the stability analysis which was discussed in Alwi & Edwards [16] applies.

Assume that $\tilde{A}^{\delta}_{21} = \tilde{\Delta}_2(t)\tilde{A}_{21}$ where $\tilde{\Delta}_2(t) \in \mathbb{R}^{n_\nu \times n_\nu}$ and $\tilde{\Delta}_2(t)$ is unknown but bounded. Also assume that $\tilde{A}^{\delta}_{11} = \tilde{G}\tilde{\Delta}_1(t)\tilde{H}$ where $\tilde{G} \in \mathbb{R}^{(n_x - n_\nu)\times n_y}$, $\tilde{H} \in \mathbb{R}^{n_y \times (n_x - n_\nu)}$ and $\tilde{\Delta}_1(t) \in \mathbb{R}^{n_y \times n_y}$. Here, the matrices $\tilde{G}$ and $\tilde{H}$ are assumed to be known, while $\tilde{\Delta}_1(t)$ is unknown but bounded. Therefore (27) can be represented by

$$\dot{\hat{e}}_1(t) = ((\tilde{A}_{11} + \tilde{G}\tilde{\Delta}_1\tilde{H}) - B_1 B_2^N B_2^+ (I + M B_1 B_2^N B_2^+)^{-1}(I_l + \tilde{\Delta}_2)\tilde{A}_{21})\hat{e}_1(t) \tag{28}$$

To facilitate the subsequent analysis, define

$$\tilde{P}(s) := \left[\begin{array}{c|cc} \tilde{A}_{11} & \tilde{G} & -B_1 B_2^N \\ \hline \tilde{H} & & \\ \tilde{A}_{21} & \multicolumn{2}{c}{0} \end{array}\right] \tag{29}$$

where s represents the Laplace variable. By construction the transfer function $\tilde{P}(s)$ is stable. Suppose

$$\gamma_1 := \|M B_1 B_2^N\| \tag{30}$$

and assume that M has been designed so that $\tilde{A}_{11} = (\hat{A}_{11} - \hat{A}_{12}M)$ is stable and $\gamma_1 \leq \frac{1}{\gamma_0}$ where γ_0 is defined in (20). Suppose that

$$\|I + \tilde{\Delta}_2(t)\| \leq \gamma_3 \tag{31}$$

where $\gamma_3 > 1$ is a known scalar. Therefore it can be shown that

$$\|B_2^+(I + M B_1 B_2^N B_2^+)^{-1}(I + \tilde{\Delta}_2)\| \leq \|B_2^+\|\|(I + M B_1 B_2^N B_2^+)^{-1}\|\|(I + \tilde{\Delta}_2)\|\| \leq \frac{\gamma_0\gamma_3}{1 - \gamma_1\gamma_0} \tag{32}$$

since $\|(I + M B_1 B_2^N B_2^+)^{-1}\| \leq (1 - \|M B_1 B_2^N\|\|B_2^+\|)^{-1} \leq (1 - \gamma_1\gamma_0)^{-1}$. Scale $\tilde{G}$ and $\tilde{H}$ appropriately so that

$$\max_{\tilde{\Delta}_1} \|\tilde{\Delta}_1(t)\| = \frac{\gamma_0\gamma_3}{1 - \gamma_1\gamma_0} \tag{33}$$

Let

$$\tilde{\Delta}(t) := \left[\begin{array}{c|c} \tilde{\Delta}_1 & 0 \\ \hline 0 & B_2^+(I + M B_1 B_2^N B_2^+)^{-1}(I + \tilde{\Delta}_2) \end{array}\right] \tag{34}$$

and so by construction $\tilde{\Delta}(t)$ from (34) satisfies

$$\|\tilde{\Delta}(t)\| < \frac{\gamma_0\gamma_3}{1 - \gamma_1\gamma_0} \tag{35}$$

Proposition 1: During a fault or failure condition, for any combinations of $0 < w_i \leq 1$, the closed-loop system will be stable if

$$0 < \frac{\gamma_2\gamma_0\gamma_3}{1 - \gamma_1\gamma_0} < 1 \tag{36}$$

where

$$\gamma_2 = \|\tilde{P}(s)\|_\infty \tag{37}$$

Proof: Consider the reduced order system from equation (28) rewritten as follows:

$$\dot{\hat{e}}_1(t) = \tilde{A}_{11}\hat{e}_1(t) + \left[\begin{array}{cc} \tilde{G} & -B_1 B_2^N \end{array}\right]\tilde{u}(t) \tag{38}$$

$$\tilde{y}(t) = \left[\begin{array}{c} \tilde{H} \\ \tilde{A}_{21} \end{array}\right]\hat{e}_1(t) \tag{39}$$

where

$$\tilde{u}(t) := \tilde{\Delta}(t)\tilde{y}(t) \tag{40}$$

Then clearly

$$\tilde{y}(s) = \tilde{P}(s)\tilde{u}(s) \tag{41}$$

where $\tilde{P}(s)$ is defined in (29) and from the Small Gain Theorem (Khalil [47]), if

$$\|\tilde{P}(s)\|_\infty \|\tilde{\Delta}(s)\| < 1 \tag{42}$$

then closed-loop system (38)-(41) is stable. Using (35) and (29), yields

$$\|\tilde{P}(s)\|_\infty \|\tilde{\Delta}(s)\| < \frac{\gamma_2\gamma_0\gamma_3}{1-\gamma_1\gamma_0} \tag{43}$$

and so if (36) holds, then from inequality (43) the small gain condition (42) is satisfied and the proposition is proved. ■

Remark: The γ_1 and γ_2 depend on the particular choice of the sliding surface matrix M. Crucially though, they do not dependent on the weight W. Conversely γ_0 depends on W but not on the design matrix M. The scalar γ_3 introduced in this paper depends on the uncertainty in the system matrix when structural damage occurs. Equation (36) represents a test to guarantee the stability of the closed-loop system when faults occur (i.e. when the w_i vary). One important feature is that in order for (26) to hold, the norm of the pseudo-inverse B_2^+ which depends on W must be bounded for all $0 < w_i \leq 1$ (which is shown in (20) and was proved in Alwi & Edwards [16] and Stewart [46]).

For a given design of hyperplane, γ_1 and γ_2 are fixed. The gain γ_0 is independent of the control design and depends on the faults and the input distribution matrix. The magnitude of the uncertainty γ_3 which can be tolerated must be such that

$$\gamma_3 \leq \frac{1-\gamma_1\gamma_0}{\gamma_2\gamma_0} = \frac{1}{\gamma_2}(\frac{1}{\gamma_0} - \gamma_1) \tag{44}$$

Since $\gamma_3 \geq 1$, a necessary condition is that

$$\frac{\gamma_2\gamma_0}{1-\gamma_1\gamma_0} < 1 \tag{45}$$

which is the condition in Alwi & Edwards [16].

Remark: Note that the condition $\|MB_1B_2^NB_2^+\| < 1$, which guarantees the inverse in (25) exists, holds because $\|MB_1B_2^NB_2^+\| \leq \|MB_1B_2^N\|\|B_2^+\| \leq \gamma_1\gamma_0 < 1$. The scalar γ_0 depends on W (but not on M), and can be interpreted physically as a worst case upper-bound on the change in the feedback loop gain (40)-(41) resulting from the faults. The scalar γ_1 depends on the designed M, i.e the choice of sliding surface, but is independent of W. Therefore, during the control law design cycle, if $\gamma_1\gamma_0 < 1$ is not satisfied, M which is chosen to make $\hat{A}_{11} - \hat{A}_{12}M$ stable, needs to be redesigned (for example by lowering the performance requirements).

B. A Sliding Mode Control Law

Next, a sliding mode controller will be designed based on the system in (23) with respect to the virtual control ν. The proposed control law is given by

$$\nu(t) = \nu_l(t) + \nu_n(t) \tag{46}$$

where

$$\nu_l(t) := -\tilde{A}_{21}\hat{e}_1(t) - \tilde{A}_{22}\sigma(t) + \nu_m(t) \tag{47}$$

and $\nu_m(t)$ is defined in (12). The nonlinear component is defined to be

$$\nu_n(t) := -(\rho(t)+\eta)\frac{\sigma(t)}{\|\sigma(t)\|} \quad \text{for } \sigma(t) \neq 0 \tag{48}$$

where η is a positive scalar.

Remark: During implementation, the discontinuity in the nonlinear control term $\frac{\sigma(t)}{\|\sigma(t)\|}$ has been smoothed by using a sigmoidal approximation $\frac{\sigma(t)}{\|\sigma(t)\|+\delta}$, where δ is a small fixed positive scalar (see, for example §3.7 in Edwards & Spurgeon [44]). This removes the so-called 'chattering' effect in the control signal and introduces further degrees of tuning to accommodate the actuator rate limits (especially during actuator fault or failure conditions).

It follows that the actual control which is sent to the actuators is resolved from the 'virtual control law' $\nu(t)$ (from (47)-(48)), using (4) and (5). Therefore $u(t)$, is defined as

$$u(t) = B_2^{\mathrm{T}}\nu(t) \tag{49}$$

Provided (36) is satisfied, the sliding mode controller can handle total actuator failures in the original system in the situation when $\det(B_2WB_2^{\mathrm{T}}) \neq 0$. Standard sliding mode controllers cannot handle total actuator failures although their inherent robustness can cope with faults.

In a fault–free situation, it is not necessary and indeed is not advisable to have a large gain on the switched term – therefore ideally the term $\rho(t)$ should adapt to the onset of a fault and react accordingly. It is easy to see from (47) that, if $y_d(t)$ is bounded, $\nu_l(t)$ is bounded by

$$\|\nu_l(t)\| < l_1\|e(t)\| + l_2 \tag{50}$$

where l_1 and l_2 are known positive constants. The gain from (48) is defined to be

$$\rho(t) = r(t)(\bar{r}_1\|e(t)\| + \bar{r}_2) \tag{51}$$

where

$$\bar{r}_1 := (\gamma_4 + (2+\gamma_1)l_1), \quad \bar{r}_2 := (\gamma_5 + (2+\gamma_1)l_2) \tag{52}$$

and the constants γ_4 and γ_5 are defined as

$$\gamma_4 := \|\tilde{A}_2^{\delta}T_\sigma T_r\|, \quad \|A_2^{\delta}\tilde{x}_m\| \leq \gamma_5 \tag{53}$$

where A_2^{δ}, T_σ and T_r are defined in (24), (22) and (15) respectively. The scalar variable $r(t)$ is an adaptive gain which varies according to

$$\dot{r}(t) = a\Big(\bar{r}_1\|e(t)\| + \bar{r}_2\Big)D_\epsilon(\|\sigma(t)\|) - br(t) \tag{54}$$

where $r(0) = 0$ and the a and b are positive design constants. The function $D_\epsilon : \mathbb{R} \mapsto \mathbb{R}$ is the nonlinear function

$$D_\epsilon(\|\sigma\|) = \begin{cases} 0 & \text{if } \|\sigma\| < \epsilon \\ \|\sigma\| & \text{otherwise} \end{cases} \tag{55}$$

where ϵ is a positive scalar. Here, ϵ is fixed to be small and helps define a boundary layer about the surface $\mathcal{S}$, inside which an acceptably close approximation to ideal sliding takes place. Provided the states evolve with time inside the boundary layer, no adaptation of the switching gains takes place. If a fault occurs, which starts to make the sliding motion degrade so that the states evolve outside the boundary layer i.e. $\|\sigma(t)\| > \epsilon$, then the dynamic coefficients $r(t)$ increase in magnitude, (according to (54)), to force the states back into the boundary layer around the sliding surface. The choice of the design parameters η, a, b and ϵ depends on the closed-loop performance specifications and requires some design iteration. The choice of these design parameters will be discussed further in Section V. The following proposition will show that $r(t)$ is bounded and motion inside a boundary layer around $\mathcal{S}$ is obtained.

Define $\mathcal{W}$ to be the set of faults such that

$$\mathcal{W} = \{(w_1 \dots w_{n_u}) \in \underbrace{[0,1] \times [0,1] \dots \times [0,1]}_{n_u \text{ times}} \;\; | \;\; \underline{\lambda}(B_2WB_2^{\mathrm{T}}) := w > 0\} \tag{56}$$

where w is a strictly positive scalar and $\underline{\lambda}(B_2WB_2^{\mathrm{T}})$ represents the smallest eigenvalue of $(B_2WB_2^{\mathrm{T}})$. Notice that $(w_1, \dots w_{n_u}) \in \mathcal{W} \Rightarrow \det(B_2WB_2^{\mathrm{T}}) \neq 0$.

Proposition 2: Consider the potentially faulty system represented by (1) with the control law in (47)-(48); then the adaptive gain $r(t)$ from (51)-(55) remains bounded, and the switching states $\sigma(t)$ enter a boundary layer around $\mathcal{S}$ in finite time for any fault condition $(w_1 \dots w_{n_u}) \in \mathcal{W}$.

Proof: See appendix. ■

Remark: Close approximation to ideal sliding can be maintained even in the presence of faults for an appropriate choice of a, b and ϵ. If ϵ=0 and b=0, it follows that $\dot{V} \leq -w^2\|\sigma\|(1-\gamma_1\gamma_0)\eta$, which means that ideal sliding can be attained and maintained in finite time. However $\epsilon = 0$ is not a practical choice, since in the presence of noise for example, $r(t)$ may become unbounded.

V. Controller design

The main objective of the controller design is to bring the damaged EL-AL 1862 aircraft to a near landing condition on Runway 27 at Schiphol airport (through a proper landing approach using localizer (LOC) and glide slope (GS) capture procedures). It is assumed that no FDI or fault reconstruction is available which replicates the actual EL-AL 1862 scenario – the flight crew were even unaware that engines no. 3 and 4 had detached from the right wing.

A linearization of the nominal aircraft has been obtained around an operating condition of 263×10^3Kg (560×10^3lbs), 92.6m/s (180kts) true airspeed, and an altitude of 600m (2000ft) at 25.6% of maximum thrust and at a 20° flap position. The result is a 12th order linear model (separated into two 6th order models) associated with the lateral and longitudinal states. For design purposes, only the four longitudinal ($x_{long} = [q\ V_{tas}\ \alpha\ \theta]^{\mathrm{T}}$) and lateral states ($x_{lat} = [p\ r\ \beta\ \phi]^{\mathrm{T}}$) have been retained. The lateral control surfaces are

$$\delta_{lat} = [\delta_{air}\ \delta_{ail}\ \delta_{aor}\ \delta_{aol}\ \delta_{sp1-4}\ \delta_{sp5}\ \delta_{sp8}\ \delta_{sp9-12}\ \delta_r\ e_{1_{lat}}\ e_{2_{lat}}\ e_{3_{lat}}\ e_{4_{lat}}]^{\mathrm{T}}$$

which represent aileron deflection (right & left - inboard & outboard)(rad), spoiler deflections (left: 1-4 & 5 & right: 8 & 9-12) (rad), rudder deflection (rad) and lateral engine pressure ratios (EPR). The longitudinal control surfaces are $\delta_{long} = [\delta_e\ \delta_s\ e_{1_{long}}\ e_{2_{long}}\ e_{3_{long}}\ e_{4_{long}}]^{\mathrm{T}}$ which represent elevator deflection (rad), horizontal stabilizer deflection (rad), and longitudinal EPR.

The controlled outputs represent the states roll (ϕ) and sideslip angle (β) for lateral control, and flight path angle (FPA) and speed (V_{tas}) for longitudinal control. These linear models of the *nominal damage free aircraft* will be used to design the control schemes which will be described in the next sections. This is a major difference compared to Maciejowski & Jones [9] where the MPC controller is designed based on exact knowledge of the post–damage aircraft.

In the original coordinates, the linear component of the control law can be summarized as:

$$\nu_l(t) = Le(t) + Fx_m(t) + Gy_d(t)$$

where $L = -SA$ and SB_ν has been scaled so that $SB_\nu = I$. The nonlinear term $\nu_n(t)$ is given in (48), where the nonlinear gain $\rho(t)$ is based on the adaptive law (51)-(55).

A. Lateral Controller Design

The feedback matrices for the ideal lateral model from (12) have been designed using eigenstructure assignment (Liu & Patton [48]). The eigenvalues were chosen as $\{-0.3500 \pm 0.1500, -0.5000, -0.4000\}$ and the desired and obtained eigenstructures are respectively

$$\underbrace{\begin{bmatrix} *+*i & *-*i & * & 0 \\ 0 & 0 & 0 & 0 \\ *+*i & *-*i & 0 & 0 \\ 1+*i & 1-*i & 1 & 1 \end{bmatrix}}_{desired} \Longrightarrow \underbrace{\begin{bmatrix} 0.3195-0.1369i & 0.3195+0.1369i & 0.4498 & 0.3748 \\ -0.0000-0.0000i & -0.0000+0.0000i & -0.0430 & -0.0526 \\ 0.1619+0.1412i & 0.1619-0.1412i & 0.0182 & 0.0275 \\ -0.9127 & -0.9127 & -0.8919 & -0.9252 \end{bmatrix}}_{obtained}$$

The feed-forward matrix G_{lat} has been designed using the inverse steady-state gain for the virtual triple $(A_{lat}, B_{\nu_{lat}}, C_{c_{lat}})$: specifically $G_{lat} = -(C_{c_{lat}}(A_{lat} + B_{\nu_{lat}}F_{lat})^{-1}B_{\nu_{lat}})^{-1}$.

It will be assumed that at least one of the control surfaces for both ϕ and β tracking will be available when a fault or failure occurs (i.e. one of either the four ailerons or the four spoilers will be available, and one of either the rudder or the four engine thrusts are available). Under these assumptions, a numerical search yields that the scalar from (20) is $\gamma_{0_{lat}} = 8.1314$.

Next, the matrix M which defines the hyperplane must be computed so that the conditions of (36) are satisfied. Here a quadratic optimal design (Edwards & Spurgeon [44]) has been used to obtain S_{lat} (which depends on the

matrix M_{lat} in equation (21)). The state weighting matrix has been chosen as $Q_{lat} = diag(2, 2, 1, 1)$. The poles associated with the reduced order sliding motion are $\{-0.7136 \pm 0.0522i\}$ and the associated natural frequency and damping ratio are 0.7155 and 0.9973 respectively. Based on M_{lat}, it can be shown that $\gamma_{1_{lat}}$ from (30) satisfies $\gamma_{1_{lat}} = 0.0230$. Consequently $\gamma_{0_{lat}}\gamma_{1_{lat}} = 0.1870 < 1$ and the requirements of (36) are satisfied. For the case of the EL-AL 1862 scenario, and by using $\tilde{G}_{lat} = 0.001I_2$ and $\tilde{H}_{lat} = I_2$ (which allows perturbations in all elements of $\tilde{A}_{11}$), it was found that the norm from (31) is $\gamma_{3_{lat}} = 1.5134$.

Finally, it can be verified that the $\mathcal{H}_\infty$ norm from (37) is $\|\tilde{P}_{lat}(s)\|_\infty = \gamma_{2_{lat}} = 0.0589$. Therefore from (36),

$$\frac{\gamma_{2_{lat}}\gamma_{0_{lat}}\gamma_{3_{lat}}}{1 - \gamma_{1_{lat}}\gamma_{0_{lat}}} = 0.8916 < 1$$

which shows that the system is stable for all $0 < w_i \leq 1$. For implementation, the discontinuity in the nonlinear control term in (48) has been smoothed by using a sigmoidal approximation $\nu^{\delta}_{n,lat} = \frac{\sigma_{lat}}{\|\sigma_{lat}\|+\delta_{lat}}$ where the scalar $\delta_{lat} = 0.05$. This introduces further degrees of freedom to accommodate actuator rate limits.

For simplicity, the variables related to the adaptive nonlinear gain have been chosen as $\bar{r}_{1_{lat}} = 0$ and $\bar{r}_{2_{lat}} = 1$. The parameter η_{lat} from (48) was chosen as $\eta_{lat} = 1$. In practice, a maximum limit ρ_{max} for the adaptive nonlinear gain in (51) has been imposed to avoid the actuators becoming too aggressive. Here, the maximum gain was set at $\rho_{max_{lat}} = 5$. The adaptation parameters from (54) have been chosen as $a_{lat} = 100, b_{lat} = 0.01$ and $\epsilon_{lat} = 5 \times 10^{-2}$. The parameter ϵ_{lat} was chosen to be able to tolerate the variation in $\|\sigma_{lat}(t)\|$ due to normal changes in flight conditions, but small enough to enable the adaptive gain to be sensitive to deviations from zero due to faults or failures. Here a_{lat} has been chosen to be large to enable small changes in $\|\sigma_{lat}(t)\|$ to cause significant changes in the gain, so that the control system reacts quickly to a fault. The parameter b_{lat} on the other hand dictates the rate at which $\rho_{lat}(t)$ will decrease after $\|\sigma_{lat}(t)\|$ has returned below the threshold ϵ_{lat}.

To emulate real aircraft flight control capability, an outer-loop heading control law was designed based on a PID, to provide a roll command to the inner-loop sliding mode controller. In the SIMONA implementation, this outer-loop heading control can be activated by a switch in the cockpit. The proportional gain as $K_{p_{lat}} = 3$, the integrator gain was set as $K_{i_{lat}} = 0.1$ and the derivative gain was set as $K_{d_{lat}} = 3$. Note that the integrator component is only activated when the heading angle error is less than 5° to remove unwanted oscillation during manoeuvres but to still eliminate steady state error.

B. Longitudinal Controller Design

As in the lateral controller, the feedback matrices for the ideal longitudinal model from (12) have been designed using eigenstructure assignment. The eigenvalues were chosen as $\{-0.2400 \pm 0.1700, -0.7000, -0.1250\}$ and the desired and obtained eigenstructures are

$$\underbrace{\begin{bmatrix} 0.5+*i & 0.5-*i & 0 & 0 \\ 0 & 0 & 0 & 1 \\ 0.5+*i & 0.5-*i & 0 & 0 \\ 0 & 0 & 1 & 0 \end{bmatrix}}_{desired} \Longrightarrow \underbrace{\begin{bmatrix} 0.1812-0.1283i & 0.1812+0.1283i & -0.1057 & 0.0001 \\ -0.0020+0.0015i & -0.0020-0.0015i & -0.0060 & 1.0000 \\ 0.3220-0.5264i & 0.3220+0.5264i & 0.9829 & -0.0037 \\ -0.7549 & -0.7549 & 0.1510 & -0.0012 \end{bmatrix}}_{obtained}$$

As in the lateral control design, the feed-forward matrix G_{long} has been designed using the inverse steady-state gain for the virtual triple so that $G_{long} = -(C_{c_{long}}(A_{long} + B_{\nu_{long}}F_{long})^{-1}B_{\nu_{long}})^{-1}$.

It will be assumed that at least one of the control surfaces for FPA tracking will still be available when a fault or failure occurs. It is also assumed that at least one of the four engines is available for V_{tas} tracking. Under these assumptions, a numerical search yields $\gamma_{0_{long}} = 8.2913$.

As in the lateral controller, a quadratic optimal design has been used to obtain the sliding surface matrix. The weighting matrix defining the cost has been chosen as $Q_{long} = diag(2, 2, 1, 1)$. The poles associated with the sliding motion can be shown to be $\{-1.1157, -0.3737\}$ (the associated natural frequencies and damping ratios are 0.6457 and 1.1533 respectively). For this choice of surface, it can be shown that $\gamma_{1_{long}} = 3.0160 \times 10^{-4}$ and $\gamma_{0_{long}}\gamma_{1_{long}} = 0.0025 < 1$. Consequently, the requirements of equation (36) are satisfied. For the case of the EL-AL 1862 scenario, with $\tilde{G}_{long} = 0.001I_2$ and $\tilde{H}_{long} = I_2$, the norm from (31) is $\gamma_{3_{long}} = 1.3842$. Finally it can be shown that the $\mathcal{H}_\infty$ norm from (37) is $\|\tilde{P}_{long}(s)\|_\infty = \gamma_{2_{long}} = 0.0115$. Consequently from (36),

$$\frac{\gamma_{2_{long}}\gamma_{0_{long}}\gamma_{3_{long}}}{1 - \gamma_{1_{long}}\gamma_{0_{long}}} = 0.1319 < 1$$

This shows that the system is stable for all $0 < w_i \leq 1$. The discontinuity in the nonlinear control term in (48) has been smoothed by using a sigmoidal approximation $\nu^{\delta}_{n,long} = \frac{\sigma_{long}}{\|\sigma_{long}\|+\delta_{long}}$ where the scalar $\delta_{long} = 0.05$.

As in the lateral design, the variables related to the adaptive nonlinear gain have been chosen as $\bar{r}_{1_{long}} = 0$ and $\bar{r}_{2_{long}} = 1$. This was also found to give sufficiently good performance and removes the dependence of $r(t)$ on $e(t)$ and simplifies the implementation. The parameter η_{long} from (48) was chosen as $\eta_{long} = 1$. In practice, a maximum limit ρ_{max} for the adaptive nonlinear gain in (51) is imposed to avoid the actuators from becoming too aggressive. Here, the maximum gain was set as $\rho_{max_{long}} = 2$. The adaptation parameters from (54) have been chosen similar to those in the lateral design; i.e. $a_{long} = 100, b_{long} = 0.01$ and $\epsilon_{long} = 5 \times 10^{-2}$.

Again, to emulate real aircraft flight control capability, an outer-loop altitude control law was designed based on a PID, to provide a FPA command to the inner-loop sliding mode controller. In the SIMONA implementation, this outer-loop altitude control can be activated by a switch in the cockpit. The proportional gain was set as $K_{p_{long}} = 0.001$, the integrator gain was set as $K_{i_{long}} = 0.00004$ and the derivative gain was set as $K_{d_{long}} = 0.02$. Note that the integrator component is only activated when the altitude error is less than 15m to remove unwanted oscillation during manoeuvres but to eliminate steady state error.

As a result of the architecture employed, both the lateral and longitudinal controllers manipulate the engine EPRs. In the trials, 'control mixing' was employed, where the signals from both the lateral controller and longitudinal controller were added together before being applied to each of the engines. This is similar to the approach adopted in Burcham *et al.*[4].

Remark: In terms of the control law design, no actuator magnitude or rate saturations are accounted for explicitly. However in the evaluations on SIMONA, these effects are present. The model-reference tracking framework was purposely chosen in this paper because it does not suffer from windup problems (due to the absence of integrators). In the event a rate limit or position limit is exceeded, a difference between the expected actuator position and the commanded one occurs, which would be interpreted as a 'fault'. The robustness property of sliding mode controllers to actuator faults would then mitigate the effect of the saturation by increasing the control effort deployed in the remaining available actuators through control the allocation process, thus reducing the burden on the saturated actuator.

VI. SIMONA IMPLEMENTATION AND TEST PILOT RESULTS

The designed controller was implemented on the SIMONA flight simulator. The command inputs from the pilot are regulated through the mode control panel (MCP). In this control scheme an APP (approach) button is implemented which is engaged in order to intercept the LOC (localizer) and GS (glide slope) for the desired runway. The controller was implemented as a SIMULINK model with appropriate inputs and outputs to connect it with the SIMONA hardware, as shown in Figure 4. In Figure 4, an ILS landing capability has been added to the control loop to allow the aircraft to land on Runway 27 at Schiphol. The controller was set up to work with an Ode4 solver with a fixed time step of 0.01s. The available processing power is sufficient to run the controller in real time, i.e. within 10 ms per time step. A connection with the MCP on the flight deck enables the selection of 'control modes' e.g. altitude hold, heading select and reference values. The simulator trials were performed with the speed, altitude and heading select modes active. The pilot commands new headings, speeds or altitudes by adjusting the controls on the MCP.

Remark: The proposed controller is relatively simple since it is designed from a linearization about an operating condition. The controller presented in this paper is considered to be a 'proof of concept' to show the capabilities of combining sliding mode control and control allocation. It will be shown in the sequel that despite being designed from a linearization, the controller is able to give good performance over a relatively large flight envelope – even in the presence of very significant and damaging faults. Because it is developed from a linearization, the controller has a relatively simple structure and is not computationally intensive. This enabled the controller to be implemented on SIMONA in real-time, within the 0.01 sec update time window necessary for implementation, as described in Smaili *et al.*[27] and Stroosma *et al.*[12].

A. ILS landing

A sensor which measures the deviation from the LOC angle/beam error (which is available in typical transport aircraft) combined with the current aircraft heading are used for aligning the aircraft towards the runway. The

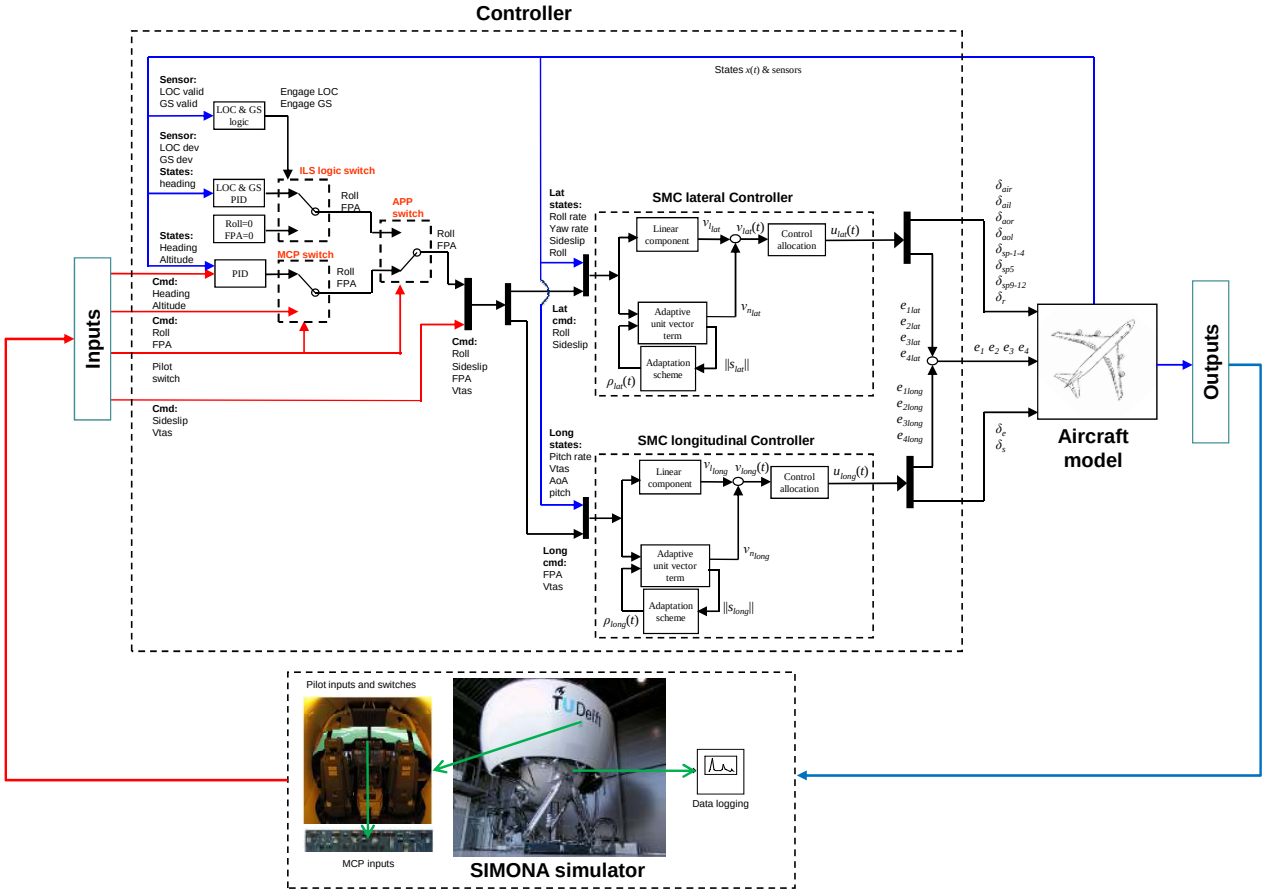

Fig. 4. SIMONA interconnections

output of this outer-loop is a roll demand for the LOC controller and an FPA demand for the GS controller. These demand signals replace the pilot's commands to the main SMC controller to allow for an almost automatic landing procedure. The outer-loop controller (LOC and GS) is armed by the pilot by engaging the APP (approach) button on the MCP when the aircraft is near the LOC signal coverage (see Figure 4 for details). In normal operation, the LOC will be the first to be engaged (LOC valid) when the aircraft is inside the LOC coverage (for this implementation, the DME is less than 46.3km when the aircraft is inside the coverage angle of $\pm 10^\circ$ from the LOC beacon and (-7°,-0.75°) inside the glideslope (GS) beacon). During the armed phase, the LOC controller is in standby mode and the aircraft is controlled either by heading or roll commands from the pilot. When the LOC is engaged (LOC valid), the LOC controller will provide the inner roll command to the core lateral sliding mode controller and the whole process becomes an automatic landing mode: i.e. no input from the pilot is needed. The GS is then engaged (GS valid) when the aircraft is inside the GS coverage (i.e. the DME is less than 18.5km, LOC is within $\pm 8^\circ$ and the GS is within (-1.35°,-5.25°) inside coverage). The GS is in an armed phase (after the APP button is engaged), and the GS controller is in a standby mode with the aircraft controlled using altitude or via FPA commands from the pilot. When the GS controller is engaged (GS valid), the GS controller will provide the FPA command to the core longitudinal SMC controller: again no input from the pilot is needed. If for some reason, during the LOC and GS manoeuvre to the runway, the LOC or GS becomes invalid (i.e. if the aircraft goes outside the LOC and GS coverage 'cones'), the outer-loop controller commands revert to heading and altitude hold (and the LOC and GS controller provide zero roll and FPA commands respectively: see Figure 4). Then, the pilot can retake full control of the aircraft by disengaging the APP mode.

Note that the reference command for ϕ was limited to 15°, and a 0° reference was applied for β to force a slide-slip free flight. As described in Lombaerts *et al.*[11], a post-failure safe flight envelope analysis suggests that a safe roll manoeuvre can only be achieved for demand values less than 20°. However, it can be argued that based on the current controller implemented in the B747, the roll reference from the autopilot is limited for passenger

comfort, and especially for LOC turning manoeuvres during the final stages of all ILS landings. Having conservative roll capabilities is a plausible predesign assumption, when designing controllers for faults or failure conditions.

B. SIMONA flight simulator results with experienced pilots

The controller has been flown by three different pilots (airline and test pilots) with experience on B747, B767, A330 and Citation II aircraft. An experienced B767 and Citation II pilot, had rigorously tested the controller during the flight evaluation campaign before the GARTEUR FM–AG16 final workshop in November 2007. During the final workshop, an experienced B747 pilot, flew the damaged 'aircraft' on the SIMONA simulator, during a presentation to the general public, including the local Dutch press (TV news, radio and newspapers). The results presented here are gained from tests flown by an experienced A330 pilot and test pilot for NLR (National Aerospace Laboratory, The Netherlands) during the pilot evaluation campaign in November 2007.

Note that even though the controller has been designed based on the linearization using a mass of approximately 263,000kg at a 20° flap position, the controller was tested with a heavy trim mass of 317,000Kg at a 1° flap position as per the actual EL-AL 1862 aircraft. This removes the advantage of low mass and low speed manoeuvrability and higher performance and controllability compared to the heavy trim mass, which was one of the main findings in Smaili & Mulder [8]. The heavy trim mass for the flight test also replicates the actual EL-AL 1862 scenario and fits with the assumption that the exact damage and condition of the aircraft, post faults, is unknown, thus making the challenge even harder.

The flight test was executed as realistically as possible. As in the actual EL-AL 1862 scenario, the aircraft flew in a northerly direction from runway 01L before starting to make a right turn. Immediately after the right turn, the EL-AL failure scenario occurs (see Figure 5) whereby engines no. 3 and 4 detached from the right wing and caused significant damage to the right wing. The objective is to fly the damaged aircraft back to the runway as intended by the crew of EL-AL 1862. The chosen runway, Runway 27, faces west at an angle of approximately 269° from the north. Therefore in order for the aircraft to land, two 90° turns must be performed before aligning the aircraft on Runway 27. During the third right turn, the aircraft is required to capture a localizer signal which guides the heading of the aircraft to line it up with the runway. During this normal procedure for landing, the aircraft will also be required to intercept a glide slope signal to enable the aircraft to descend at a 3° flight path angle, which will bring the aircraft to the landing target zone. The flare and the actual landing of the aircraft are not carried out and the simulation was stopped at a point 50 ft above ground level.

C. Classical Controller

Figure 5 shows the results of the piloted evaluation using the classical controller and proposed SMC controller. The idea of a fault–free test of the SMC is to give the pilot the feel of the capability of the controller in the nominal condition. Initially the aircraft was flown straight and level, before a heading change of 90° to the east was performed. The pilot tested the aircraft's capability to climb to a pre-specified altitude from 600m (2000ft) altitude to approximately 800m (2500ft). Then the pilot commands a return to an altitude of 600m and performs another right turn to capture the localizer. At this stage, the pilot 'arms' the approach mode in order to prepare for an automated landing approach. Once the aircraft captures the localizer signal, a final turn towards the centre-line of Runway 27 is started, and after a while, the glide slope signal is captured and the aircraft descends towards the runway at a 3° glide slope. Note that starting from the moment the pilot activates the APP button in the MCP and the localizer signal has been captured, the aircraft is in a fully automated landing mode and no other pilot input is required.

The classical controller was also tested by the pilots to give them some 'feel' and an idea of the severity of the actual EL-AL scenario. With this controller, the pilots manually flew the aircraft using control wheel and column inputs. Piloted evaluation using the classical controller under the EL-AL 1862 scenario (Figure 5) shows that after the failure, the aircraft is still able to do right turns. Only during the final stage of the test flight does the aircraft lose control and crash before being able to line up with the runway.

Figures 6-8 show the results of the piloted evaluation using the classical controller tested under the EL-AL flight 1862 scenario.

Figure 6 shows the pilot control deflections. As described in the incident studies in Smaili & Mulder [8] and the incident report [29], similar patterns appear. Immediately after the failure, the deflection of wheel, column and

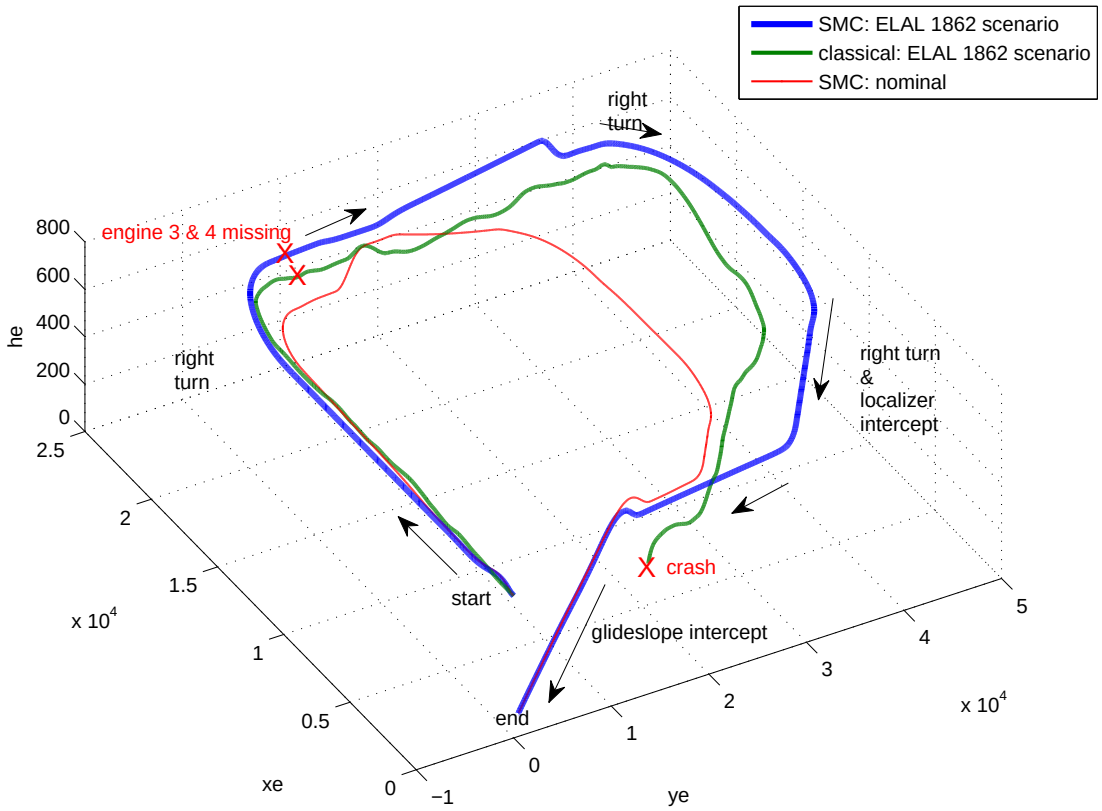

Fig. 5. Classical & SMC controller: 3-D flight trajectory

pedal increase in magnitude. As in the EL-AL 1862 flight, almost maximum wheel deflection to the left (negative) to counter the right turn is visible. Also visible is the pedal deflection to counteract the yawing moment of the asymmetric thrust. Figure 6 also shows that near to the final stages of the test, a flap setting of 1° is selected to prepare for landing. At about 600s, the power lever angle (throttle) is also reduced for landing. However, when the speed reaches 110m/s (approx 220Kts) near 700s (Figure 7), the aircraft becomes hard to control and banks to the right. Figure 6 shows that maximum left (negative) pilot wheel deflection is applied. Still unable to recover from the right bank, the flap is returned to a 0° setting, and the throttle input is increased in order to regain control. However the aircraft still rolls to the right and loses altitude and speed. The loss of altitude and FPA tries to be compensated for by the high positive (pull towards the pilot) column deflection. At this stage, all control is lost and the aircraft rolls at almost 80° right with the FPA nearing -40° and the pitch angle passing -20°. This is similar to what is described in the incident report in [29] when the EL-AL 1862 aircraft hit the apartment building in Bijlmermeer, Amsterdam.

Analyzing the plots further, it can be seen that when the throttle is reduced in preparation for landing, the speed becomes low, and during descent, the angle of attack becomes high. As discussed in incident report [29] and Smaili *et al.*[8], [27], [8], the increase in the angle of attack causes (high) flow separation and turbulence behind the damaged right wing leading edge, resulting in the loss of lift and drag rise (compared to the left wing). This increases the rolling and yawing moment to the right and a further drop in altitude and speed.

Figure 8 shows the control surface deflections of the classical controller. One major feature of the classical controller is that most of the control surfaces are mechanically linked. For example, the outboard ailerons on the left and right wing are only fully active when a flap setting of more than 5° is used (Hanke & Nordwall [49] and Hanke [50]). This can be seen in Figure 8, where the outboard aileron is inactive (0° deflection) throughout the flight test. The large deflection of the left aileron and spoilers up to the saturation limits (-20° for the aileron and 40° for the spoiler) after the engine failure shows that there is limited control even at a speed of 130-140kts. Note that a positive deflection for ailerons is a deflection down, and for the spoilers, positive is deflected up (Hanke & Nordwall [49] and Hanke [50]). Figure 8 shows that the aileron deflections are most of the time at the saturation limits after the loss of engines 3 and 4 to provide enough roll moment in order to obtain straight and level flight,

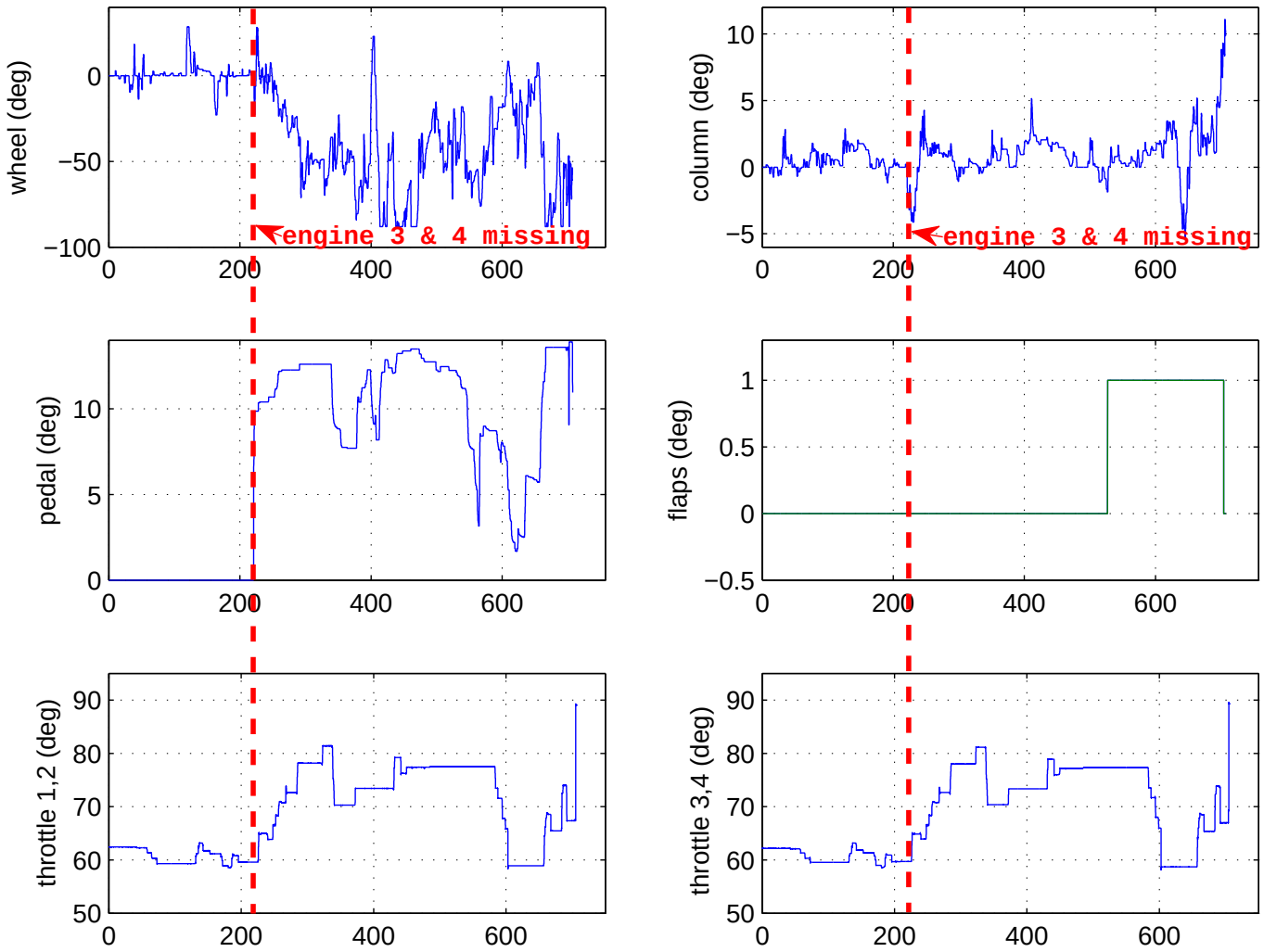

Fig. 6. EL-AL 1862 scenario: classical controller: pilot deflection

and therefore most of the roll manoeuvre capability is assisted by the left spoiler deflections. Shortly after the reduction in speed i.e. approximately after 600s, the left aileron and spoilers saturate again, but due to the lower speed and higher angle of attack, the control surface deflections are insufficient to regain control as the aircraft has gone beyond the capability of the control surfaces to provide enough roll moment. Note that the general control surface deflections and behaviour in Figures 6-8 closely follow the findings of the actual EL-AL 1862 incident reported by the Netherlands Aviation Safety Board [29].

Figure 5 shows the flight trajectory of the test. Three different trajectories are shown; the EL-AL 1862 scenario with classical and SMC controllers and one with the SMC without any failure. With the classical controller, the pilot manages to maintain some performance and managed two banking turn manoeuvres. During the preparation for landing and capture of the localizer, the aircraft loses control and the simulation was stopped. The other two trajectories associated with safe landings by the SMC controller will be discussed in the next section.

D. SMC controller

As discussed in Section V, the controller has been designed based on a linearization obtained around an operating condition of 263×10^3Kg (580×10^3lbs), 92.6m/s (180kts) true airspeed, and an altitude of 600m (2000ft) at 25.6% of maximum thrust and at a 20° flap position. The actual pilot tests were performed at 317×10^3Kg (700×10^3lbs), a speed of 133.8m/s (260kts) and a flap setting of 1°. The tests were deliberately undertaken at a different trim condition to allow the pilot to rigorously test the controller and access its performance under different operating conditions.

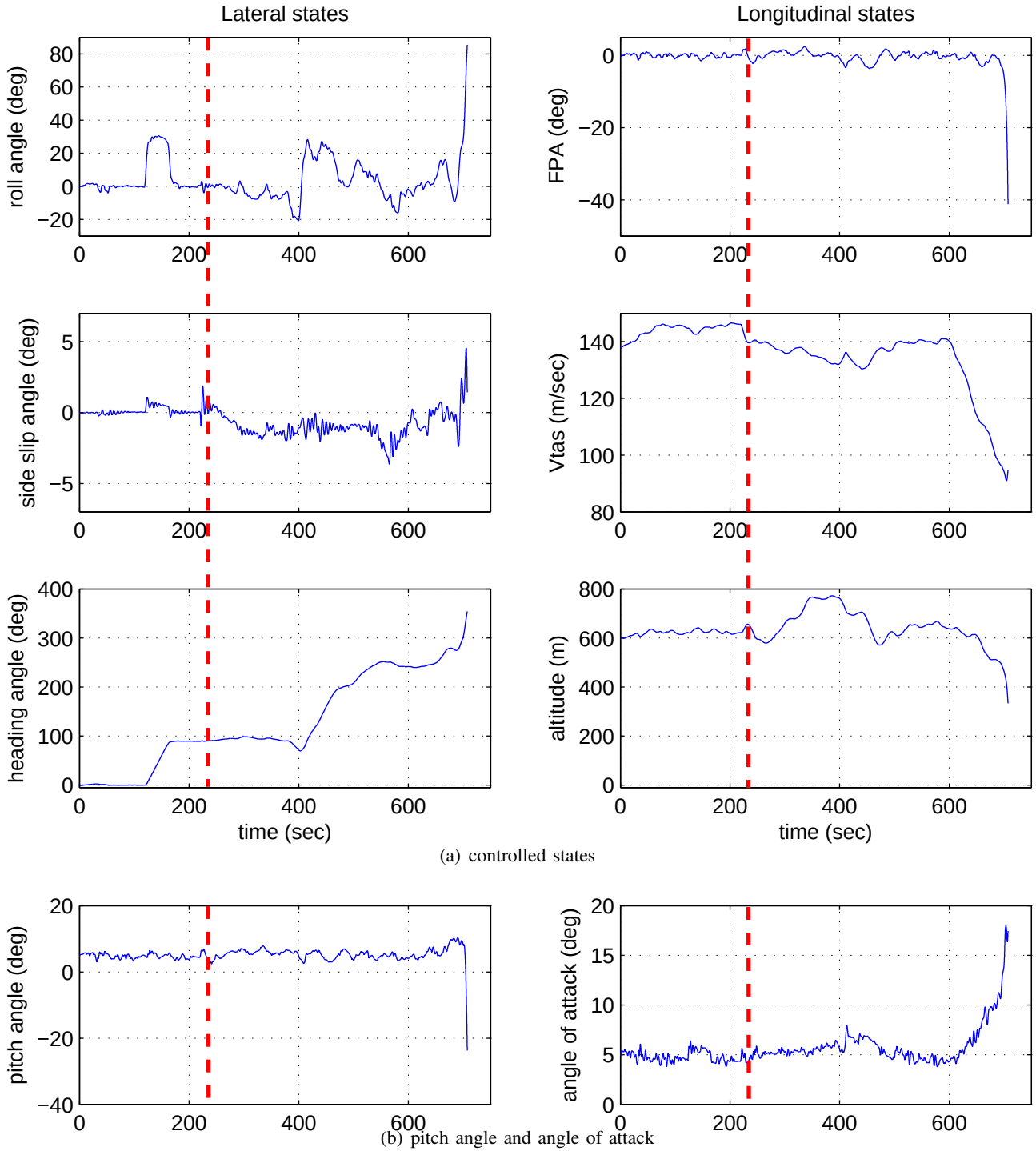

(a) controlled states

(b) pitch angle and angle of attack

Fig. 7. EL-AL 1862 scenario: classical controller: states

Note that for the purpose of testing the modern control strategy for fault tolerant control, the large transport aircraft setup in the GARTEUR FM–AG16 program using the FTLAB747 software, has been modified to include a state of the art fly by wire capability 'removing' mechanical links and locks from the classical B747 configuration (Smaili *et al.*[27]). This allows more flexibility in the control strategy exploiting independent control of all available surfaces thus increasing the ways redundant control surfaces can be used to achieve fault tolerant control.

Figure 5 also shows the trajectory of the SMC controller tested with the EL-AL 1862 failure scenario. The same controller as that used in the nominal fault–free case is applied. In general, the controller performs the same right

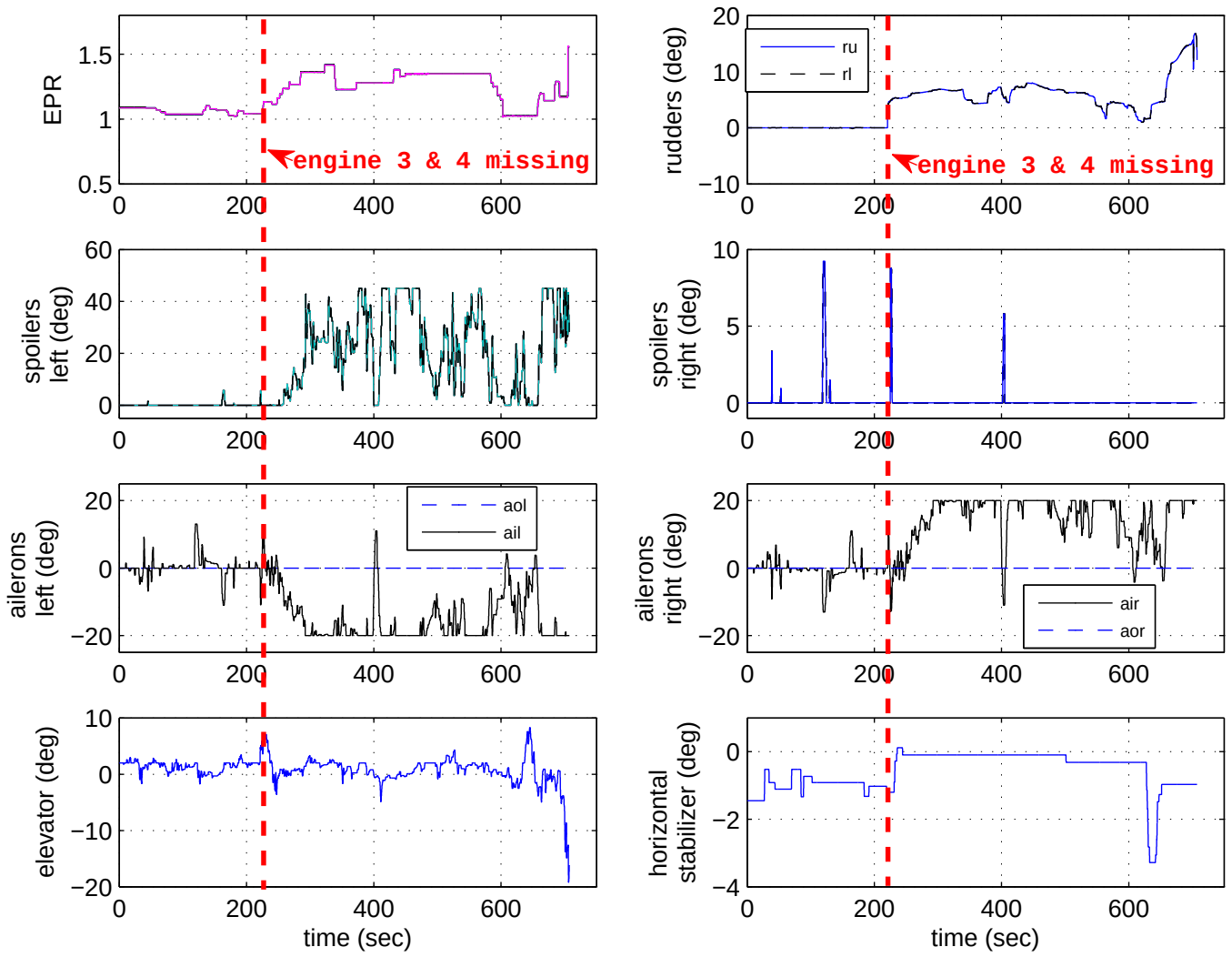

Fig. 8. EL-AL 1862 scenario: classical controller: control surfaces deflection

turn manoeuvres, LOC and GS intercept and lands on Runway 27. The SMC with the EL-AL 1862 failure manage to bring the aircraft near to landing on the desired runway. Figure 9 shows the controlled states of the damaged aircraft with the SMC controller. Note at the beginning of the simulation, before the failure occurs at around 200s, the FPA, Vtas and altitude show small steady state errors due to the mismatch between the designed trim conditions and the test conditions as described earlier. This is due to the absence of integrators in the main SMC controller. The mismatch between the designed and test trim conditions demonstrate the controller coping with uncertainty and allows the pilot to rigorously test the controller outside its 'comfort zone'.

Figure 9 shows that after the failure occurs, at approximately 200s, the climb capability of the aircraft is severely degraded when the pilot requests an increase in altitude to 800m (from 600m). On the other hand, the more important descent capability of the SMC controller is not degraded as it is able to follow the glide slope of 3° towards the runway. This is shown in Figure 10. The glide slope error is maintained below 0.5°. Figure 9 shows that the side slip angle of the damaged aircraft has been maintained in the interval (0.5°,-1.5°) which is an improvement on the classical controller (as flown by the pilot) in Figure 9. Heading changes of the damaged aircraft with the SMC controller in Figure 9 also show a more systematic and higher level of performance of the controller – even when subjected to the EL-AL 1862 failures. This shows that the lateral controller is able to deal with the asymmetrical thrust condition, extensive wing damage and control surface loss of efficiency (due to the failure of the hydraulic systems 3 and 4), and maintains the desired change in heading. Decreasing the speed (to approximately 120m/s (233.26kts)) helps in terms of lateral control (Smaili & Mulder [8] and the incident report [29]). This is due to

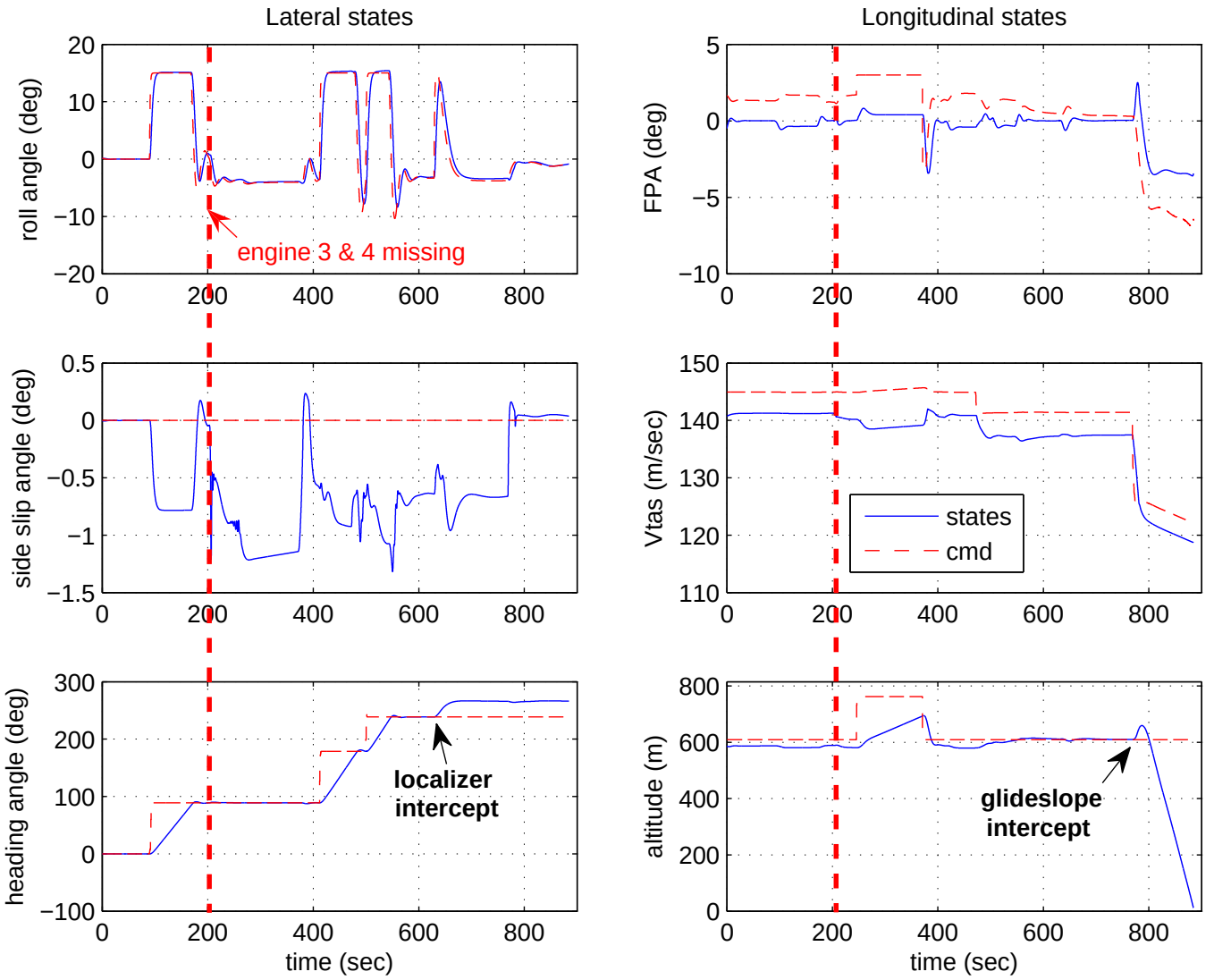

Fig. 9. EL-AL 1862 scenario: SMC controller: controlled states

the lower thrust that is required at lower speed, and thus a lower yawing moment resulting from the asymmetrical thrust condition. This is seen in terms of the deviation of the side slip angle in Figure 9. The side slip angle is much smaller than at higher speed after the failure has occurred. The roll angle tracking again shows good performance even after the loss of the engines and the hydraulics associated with the EL-AL 1862 scenario.

Note that in Figure 9, the heading angle and altitude plot only show the command signals from the MCP. After the localizer and glide slope have been engaged, the heading and altitude commands from the MCP are no longer used (and remain at the set value). Instead, the heading and altitude commands come from the ILS navigation (not shown in the heading angle and altitude plot in Figure 9).

Figure 10 shows the signals from the ILS sensors. It represents the DME , LOC & GS deviation and the moment when the LOC and the GS are engaged (valid/engaged) after being 'armed' using the APP button in the MCP. As usual, the LOC is engaged before the GS. The LOC coverage is much further than the GS and this allows the aircraft to be aligned to the extended centre line of the runway before following the specified 3° glide slope descent.

Figure 11 shows the control surface deflections under the EL-AL 1862 scenario. This figure highlights the major difference between the classical controller (which is mechanically linked) and the FBW aircraft that has been provided by the GARTEUR FM–AG16 modification (Smaili *et al.*[27]). In this figure, the outboard ailerons can be seen to be independently mobile before the occurrence of the failure. After the failure, the right outboard ailerons

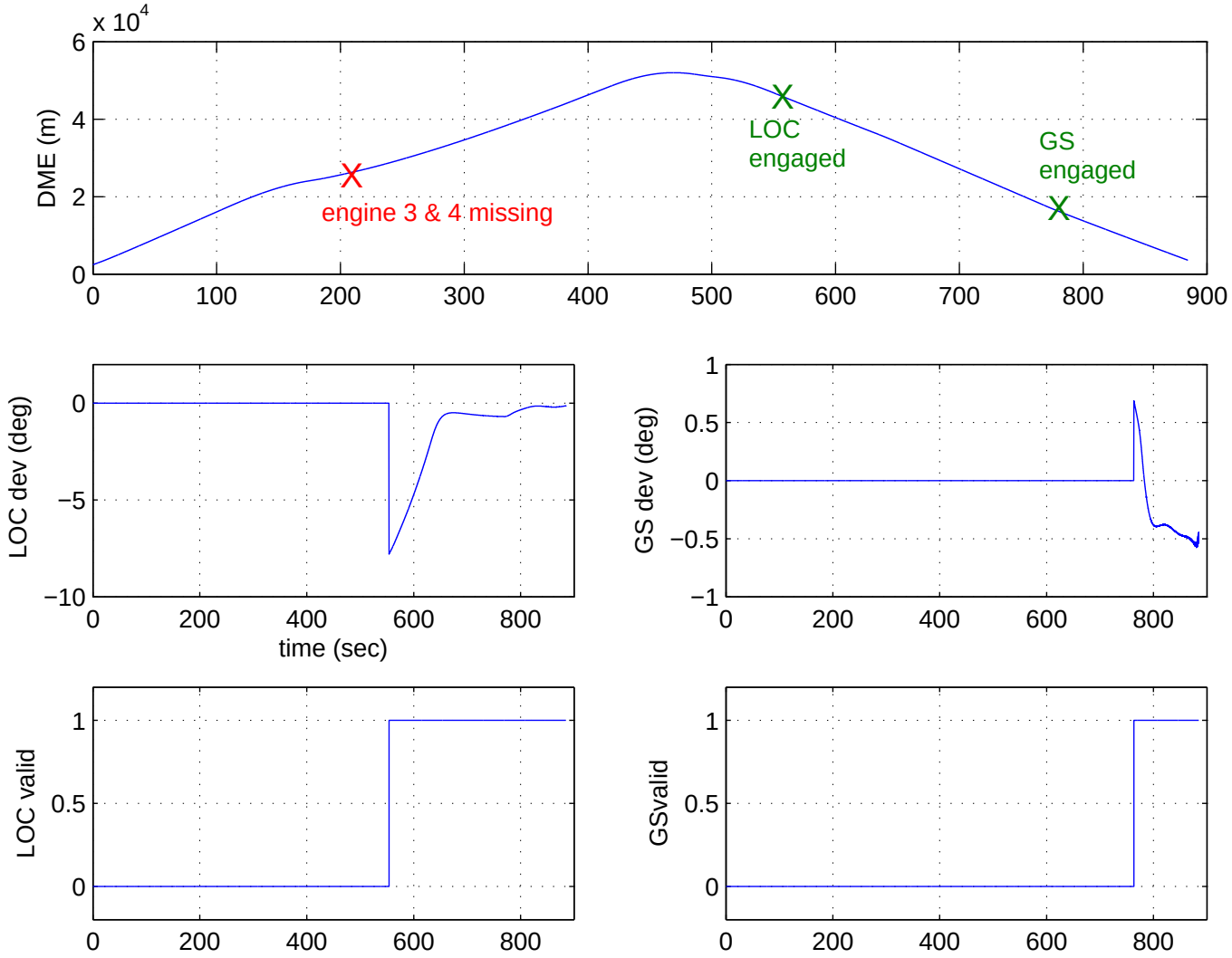

Fig. 10. EL-AL 1862 scenario: SMC controller: LOC and GS deviation angle

'float' due to the loss of hydraulic systems 3 and 4. Independent control can also be seen in the spoilers, elevators, rudders and EPR. The effect of losing the hydraulic system can also be seen in the floating of the inboard left and outboard right elevators (see Figure 11) where a clear distinction between the control surface deflection can also be seen. The spoilers also show similar patterns. Before the loss of engine 3 and 4 occurred, all the spoilers seem to be moving independently; and when the failure occurs, only spoilers 2,3,10 and 11 are active, the rest remain at zero deflection. In general, the control surface deflections of the elevators, ailerons and spoilers are almost half of the ones using the classical controller (see Figure 11). The control surface deflections from the SMC controller do not reach the saturation limits of the surfaces and the spoilers and the ailerons are generally less aggressive. Engine EPR shows that differential thrust has been used to achieve the desired performance, to obtain a small side slip angle and roll angle. Note that all the surfaces are controlled independently by the CA SMC scheme. Pilot's inputs only come from supplying the higher level commands such as heading and altitude change (or roll or FPA commands through the MCP panel). This reduces the pilot's workload in comparison with the classical controller where the demand is high.

Remark: Figure 11 shows no chattering in the lateral and longitudinal control surface deflections since the discontinuity in the nonlinear control term in (48) has been smoothed by using a sigmoidal approximation as explained in Section V. Figure 11 shows that the right outboard aileron has an up (negative) deflection due to the

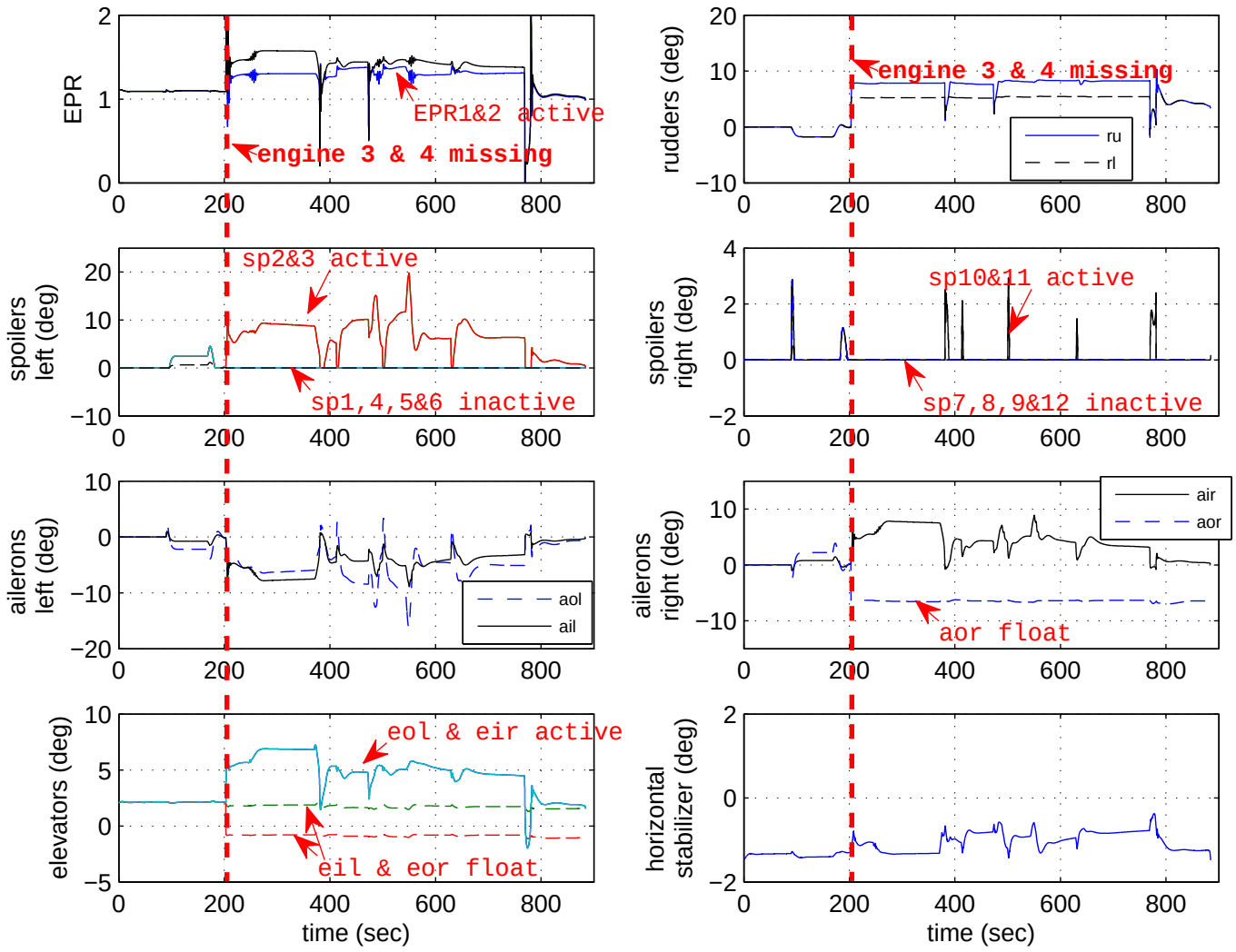

Fig. 11. EL-AL 1862 scenario: SMC controller: control surfaces deflection

'float' failure resulting from the loss of hydraulics.[9]

Note that although during the design stage, the elevator is modelled as one surface, as shown in Figure 11, the robustness property of SMC (to uncertainty in the actuator channels) and the flexibility of the CA scheme, manages to redistribute the control effort to the remaining functional elevators (i.e. the left outboard and right inboard elevators) and the stabilizer.

Figure 12(a) and 12(b) show the adaptive gain and the associated $\|\sigma(t)\|$ signals that initiate the gain adaptation. Before the occurrence of the failure, the sliding signal $\sigma(t)$ is below the selected threshold. Once the threshold is exceeded, the gain is adapted from a minimum of 1 up to the maximum of 5 and 2 for the lateral and longitudinal axes respectively. Large deviation from the sliding surface $\sigma(t) = 0$ shows the severity of the faults. After the failure has occurred and during manoeuvres, the switching function plot $\sigma(t)$ deviates away from the ideal sliding surface. However, during or near landing conditions, the switching function returns below the adaptation threshold, near to zero. During this time, the adaptive gain reduces to the minimum value of 1.

Although the SMC controller can be implemented in such a way that pilot's inputs (such as column, wheel and pedal) can also be used, the purpose here is to show that, as a proof of concept, the SMC controller is more than able to handle all the rigorous tests and failures it is subjected to using the minimal amount of input from the pilot,

[9]During a 'float' failure, (as described in Bošković and Mehra [51]) the control surface moves freely without producing any moment. In the case of straight and level flight, the floating control surface moves freely in the direction of angle of attack (Ganguli *et al.*[52]) i.e. at an up (negative) position.

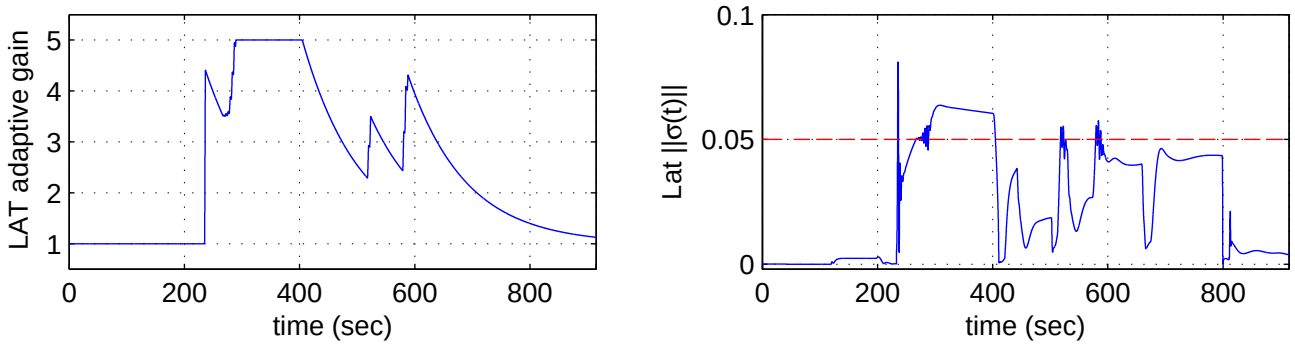

(a) lateral

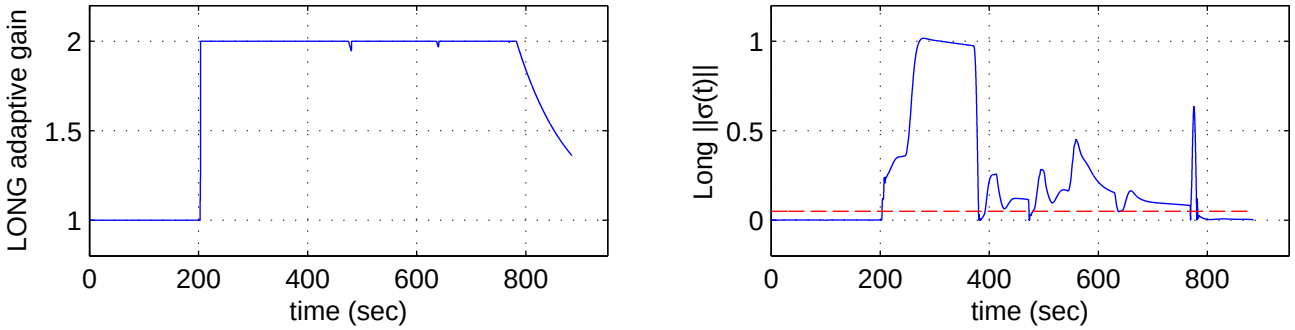

(b) longitudinal

Fig. 12. EL-AL 1862 scenario: SMC controller: adaptive gain and switching function.

thus lowering the workload during such an emergency condition. This allows the pilot to concentrate on higher level decisions.

VII. Conclusions

This paper has presented piloted flight simulator results associated with the EL-AL flight 1862 (Bijlmermeer incident) scenario which is one of the case studies of the GARTEUR FM–AG16. The results represent the successful implementation of a FTC SMC controller on the SIMONA 6-DOF flight simulator configured to represent a large transport aircraft with pilots evaluating and testing the controller. The results show that the proposed SMC scheme has the ability to position an aircraft for landing. The paper has further developed the sliding mode control allocation scheme proposed in Alwi & Edwards [16], [15] to handle the situation in which changes to the nominal system matrix occur as a result of damage to the airframe which changes the aerodynamic properties of the aircraft. A formal proof of closed-loop stability has been provided for a range of parameter variations.

Appendix

Proof of Proposition 2 : Define a scalar

$$\zeta := \frac{1}{w^2(1-\gamma_1\gamma_0)} \tag{57}$$

The expression for ζ in (57) is guaranteed to be positive, since in the requirements of equation (36), the inequality $\gamma_1\gamma_0 < 1$ must hold. Assume that $\dot{K}(t) = 0$ almost always, this implies $\dot{W}(t) = 0$ almost always and so *only isolated abrupt step changes in the effectiveness are considered here*. Using the fact that $(B_2 W B_2^{\mathrm{T}}) > 0$, the following candidate Lyapunov function

$$V = \frac{1}{2}\left(\sigma^{\mathrm{T}}(B_2 W B_2^{\mathrm{T}})\sigma + \frac{w^2}{a}(1-\gamma_1\gamma_0)(r(t)-\zeta)^2\right) \tag{58}$$

is positive definite with respect to σ, the adaptive gain error $r(t)-\zeta$, and is radially unbounded. Taking derivatives along trajectories

$$\dot{V} = \sigma^{\mathrm{T}}(B_2WB_2^{\mathrm{T}})\dot{\sigma} + \frac{w^2}{a}(1-\gamma_1\gamma_0)(r(t)-\zeta)\dot{r}(t) \tag{59}$$

From (23) (and using (46) and (47)),

$$\begin{aligned}
\dot{\sigma}(t) &= (\tilde{A}_{21}+\tilde{A}_{21}^{\delta})\hat{e}_1(t) + (\tilde{A}_{22}+\tilde{A}_{22}^{\delta})\sigma(t) + (\nu(t)-\nu_m(t)) \\
&\quad -(I - MB_1B_2^NWB_2^{\mathrm{T}} - B_2WB_2^{\mathrm{T}})\nu(t) + \tilde{A}_2^{\delta}\tilde{x}_m(t) \\
&= \tilde{A}_{21}^{\delta}\hat{e}_1(t) + \tilde{A}_{22}^{\delta}\sigma(t) + (I + MB_1B_2^NB_2^{+})(B_2WB_2^{\mathrm{T}})\nu_n(t) \\
&\quad -(I - MB_1B_2^NWB_2^{\mathrm{T}} - B_2WB_2^{\mathrm{T}})\nu_l(t) + \tilde{A}_2^{\delta}\tilde{x}_m(t) \\
&= \tilde{A}_2^{\delta}\tilde{e}(t) + \tilde{A}_2^{\delta}x_m(t) + (I + MB_1B_2^NB_2^{+})(B_2WB_2^{\mathrm{T}})\nu_n(t) \\
&\quad -(I - MB_1B_2^NWB_2^{\mathrm{T}} - B_2WB_2^{\mathrm{T}})\nu_l(t)
\end{aligned} \tag{60}$$

where $\tilde{e} = (\hat{e}_1(t), \sigma(t))$. Using the fact that

$$\|\tilde{A}_2^{\delta}\tilde{e}(t) + \tilde{A}_2^{\delta}x_m(t)\| \le \|\tilde{A}_2^{\delta}\tilde{e}(t)\| + \|\tilde{A}_2^{\delta}\tilde{x}_m(t)\| \le \underbrace{\|\tilde{A}_2^{\delta}T_{\sigma}T_r\|}_{\gamma_4}\|e(t)\| + \underbrace{\|\tilde{A}_2^{\delta}\tilde{x}_m(t)\|}_{\gamma_5} \tag{61}$$

and

$$\sigma(t)^{\mathrm{T}}(B_2WB_2^{\mathrm{T}})(B_2WB_2^{\mathrm{T}})\sigma(t) = \|B_2WB_2^{\mathrm{T}}\sigma\|^2$$

where $\|(B_2WB_2^{\mathrm{T}})\| \le \|B_2B_2^{\mathrm{T}}\| = 1$, together with the fact $\|WB_2^{\mathrm{T}}\| \le \|W\|\|B_2^{\mathrm{T}}\| \le 1$ for all $(w_1, \dots w_{n_u}) \in \mathcal{W}$, it follows that when $\sigma \neq 0$

$$\begin{aligned}
\sigma^{\mathrm{T}}(B_2WB_2^{\mathrm{T}})\dot{\sigma} &= -\frac{(\rho+\eta)}{\|\sigma\|}\|B_2WB_2^{\mathrm{T}}\sigma\|^2 - (\rho+\eta)\sigma^{\mathrm{T}}(B_2WB_2^{\mathrm{T}})(MB_1B_2^NB_2^{+})(B_2WB_2^{\mathrm{T}})\frac{\sigma}{\|\sigma\|} \\
&\quad -\sigma^{\mathrm{T}}(B_2WB_2^{\mathrm{T}})(I - MB_1B_2^NWB_2^{\mathrm{T}} - B_2WB_2^{\mathrm{T}})\nu_l(t) \\
&\quad +\sigma^{\mathrm{T}}(B_2WB_2^{\mathrm{T}})(\tilde{A}_2^{\delta}\tilde{e}(t) + \tilde{A}_2^{\delta}\tilde{x}_m(t)) \\
&\le -\frac{(\rho+\eta)}{\|\sigma\|}\|B_2WB_2^{\mathrm{T}}\sigma\|^2 + \frac{(\rho+\eta)}{\|\sigma\|}\|B_2WB_2^{\mathrm{T}}\sigma\|^2\|(MB_1B_2^NB_2^{+})\| \\
&\quad +\|B_2WB_2^{\mathrm{T}}\sigma\|\|(I - MB_1B_2^NWB_2^{\mathrm{T}} - B_2WB_2^{\mathrm{T}})\|\|\nu_l(t)\| \\
&\quad +\|B_2WB_2^{\mathrm{T}}\sigma\|\|(\tilde{A}_2^{\delta}\tilde{e}(t) + \tilde{A}_2^{\delta}\tilde{x}_m(t))\| \\
&\le \|B_2WB_2^{\mathrm{T}}\sigma\|\Big(-\frac{(\rho+\eta)}{\|\sigma\|}\|B_2WB_2^{\mathrm{T}}\sigma\|(1-\gamma_1\gamma_0) \\
&\quad +(2+\gamma_1)\|\nu_l(t)\| + (\gamma_4\|e(t)\| + \gamma_5)\Big)
\end{aligned} \tag{62}$$

since $\|MB_1B_2^NB_2^{+}\| \le \|MB_1B_2^N\|\|B_2^{+}\| \le \gamma_0\gamma_1$, and

$$\|I - MB_1B_2^NWB_2^{\mathrm{T}} - B_2WB_2^{\mathrm{T}}\| \le 1 + \|MB_1B_2^NWB_2^{\mathrm{T}}\| + \|B_2WB_2^{\mathrm{T}}\| \le 2 + \gamma_1$$

Using the Rayleigh principle, $-\|B_2WB_2^{\mathrm{T}}\sigma\|^2 \le -\underline{\lambda}(B_2WB_2^{\mathrm{T}})^2\|\sigma\|^2 = -w^2\|\sigma\|^2$. This together with the fact that $\bar{\lambda}(B_2WB_2^{\mathrm{T}}) = 1$, means inequality (62) implies

$$\begin{aligned}
\sigma^{\mathrm{T}}(B_2WB_2^{\mathrm{T}})\dot{\sigma} &\le -w^2\|\sigma\|(\rho+\eta)(1-\gamma_1\gamma_0) + \|\sigma\|(2+\gamma_1)\|\nu_l(t)\| + \|\sigma\|(\gamma_4\|e(t)\| + \gamma_5) \\
&= w^2\|\sigma\|(1-\gamma_1\gamma_0)\Big(-(\rho+\eta) + \zeta(2+\gamma_1)\|\nu_l(t)\| + \zeta(\gamma_4\|e(t)\| + \gamma_5)\Big) \\
&\le w^2\|\sigma\|(1-\gamma_1\gamma_0)\Big(-(\rho+\eta) + \zeta(2+\gamma_1)(l_1\|e(t)\| + l_2) + \zeta(\gamma_4\|e(t)\| + \gamma_5)\Big) \\
&= w^2\|\sigma\|(1-\gamma_1\gamma_0)\Big(-(\rho+\eta) + \zeta(\underbrace{\gamma_4 + (2+\gamma_1)l_1}_{\bar{r}_1})\|e(t)\| + \zeta(\underbrace{\gamma_5 + (2+\gamma_1)l_2}_{\bar{r}_2})\Big)
\end{aligned} \tag{63}$$

where ζ is defined in (57), and $\bar{r}_1$ and $\bar{r}_2$ are defined in (52). Using (50) and (51), inequality (63) above can be written as

$$\sigma^{\mathrm{T}}(B_2WB_2^{\mathrm{T}})\dot{\sigma} \le -w^2\|\sigma\|(1-\gamma_1\gamma_0)\eta - w^2\|\sigma\|(1-\gamma_1\gamma_0)(\bar{r}_1\|e(t)\| + \bar{r}_2)(r(t)-\zeta) \tag{64}$$

Finally, substituting (54) and (64) into (59) yields

$$\begin{aligned}\dot{V} \leq & -w^2\|\sigma\|(1-\gamma_1\gamma_0)\eta - w^2\|\sigma\|(1-\gamma_1\gamma_0)(\bar{r}_1\|e(t)\|+\bar{r}_2)(r(t)-\zeta) \\ & +w^2(1-\gamma_1\gamma_0)(r(t)-\zeta)\Big(\bar{r}_1\|e(t)\|+\bar{r}_2\Big)D_\epsilon(\|\sigma(t)\|) \\ & -\frac{b}{a}w^2(1-\gamma_1\gamma_0)(r(t)-\zeta)r(t) \end{aligned} \tag{65}$$

If $\|\sigma\| > \epsilon$ then $D_\epsilon(\|\sigma\|) = \|\sigma\|$ and so substituting in (65) and simplifying terms yields

$$\dot{V} \leq -w^2\|\sigma\|(1-\gamma_1\gamma_0)\eta - \frac{b}{a}w^2(1-\gamma_1\gamma_0)(r(t)-\zeta)r(t) \tag{66}$$

By construction $0 \leq \gamma_1\gamma_0 < 1$ and $r(t) \geq 0$. Further manipulation of (66), and using (57) yields

$$\dot{V} \leq -w^2\|\sigma\|(1-\gamma_1\gamma_0)\eta - \frac{b}{a}w^2(1-\gamma_1\gamma_0)(\frac{1}{2}\zeta - r)^2 + \frac{b}{4a}\frac{1}{w^2(1-\gamma_1\gamma_0)} \tag{67}$$

since expanding the quadratic term on the right-hand side of (67) gives the right-hand side of (66). If $\|\sigma\| > \epsilon$, then $w^2\|\sigma\|(1-\gamma_1\gamma_0)\eta \geq w^2(1-\gamma_1\gamma_0)\eta\epsilon$. The quantities ϵ, η, a and b are design parameters and so if they are chosen to satisfy

$$\epsilon\eta \geq \frac{b}{4a}\frac{1}{w^4(1-\gamma_1\gamma_0)^2} = \frac{b}{4a}\zeta^2 \tag{68}$$

then from (67)

$$\dot{V} \leq -\frac{b}{a}w^2(1-\gamma_1\gamma_0)(\frac{1}{2}\zeta - r)^2 \leq 0$$

If $\|\sigma\| < \epsilon$ then $D_\epsilon(\|\sigma\|) = 0$ and so substituting in (65) and simplifying terms yields

$$\begin{aligned}\dot{V} \leq & -w^2\|\sigma\|(1-\gamma_1\gamma_0)\eta - w^2\|\sigma\|(1-\gamma_1\gamma_0)(\bar{r}_1\|e(t)\|+\bar{r}_2)(r(t)-\zeta) \\ & -\frac{b}{a}w^2(1-\gamma_1\gamma_0)(r(t)-\zeta)r(t) \end{aligned} \tag{69}$$

Notice by construction $\gamma_1\gamma_0 < 1$ and $r(t) \geq 0$ and therefore for $\|\sigma\| < \epsilon$ and $r(t) > \zeta$, it follows $\dot{V} < 0$. Define a rectangle in $\mathbb{R}^2$ as

$$\mathcal{R} = \{(\|\sigma\|, r) \;\; | \;\; \|\sigma\| \leq \epsilon, \; 0 \leq r \leq \zeta\} \tag{70}$$

Also define $\mathcal{R}_+ \in \mathbb{R}^2$ as $\mathcal{R}_+ = \{(\|\sigma\|, r) \mid r \geq 0\}$. By construction of the adaptive gains, $r(t) \geq 0$ for all time and so the trajectory of $(\|\sigma(t)\|, r(t)) \in \mathcal{R}_+$ for all time, and so outside the set $\mathcal{R} \cap \mathcal{R}_+ = \mathcal{R}$, from (67) and (69), the derivative of the Lyapunov function $\dot{V} < 0$. Let $\mathcal{V}_d$ denote the truncated ellipsoid

$$\mathcal{V}_d = \{(\|\sigma\|, r) \;\; | \;\; V(\|\sigma\|, r) \leq d\} \;\cap\; \mathcal{R}_+$$

where $V(\cdot)$ is defined in (58). Because $\mathcal{R}$ in (70) is a compact set, for a given $w > 0$, there exists a unique $d_0 > 0$ such that $d_0 = \min\{d \in \mathbb{R}_+ \mid \mathcal{R} \subset \mathcal{V}_d\}$. As shown in Figure 13, since $\mathcal{R} \subset \mathcal{V}_{d_0}$, it follows outside $\mathcal{V}_{d_0}$ the derivative of the Lyapunov function $\dot{V} < 0$ and so $\mathcal{V}_{d_0}$ is an invariant set which is entered in finite time t_0. Since $\mathcal{V}_{d_0}$ is entered in finite time, $V(\|\sigma\|, r) \leq d_0$ for all $t > t_0$ which implies $\|\sigma\| \leq \sqrt{2d_0/w}$ for $t > t_0$, and hence σ enters and remains in a boundary layer of size $\sqrt{2d_0/w}$ around the ideal sliding surface $\mathcal{S}$. ■

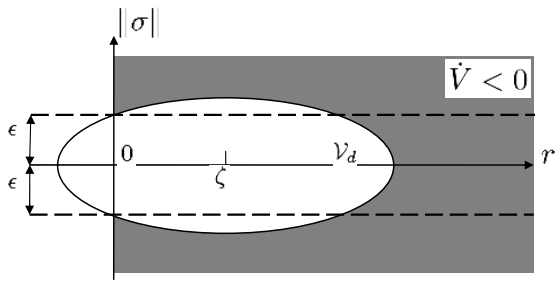

Fig. 13. Level set of the Lyapunov functions V

REFERENCES

[1] Burcham, F. W., Fullertron, C. G., and Maine, T. A., "Manual manipulaton of engine throttles for emergency flight control," Tech. Rep. NASA/TM-2004-212045, NASA, 2004.

[2] Gero, D., *Aviation disasters : the world's major civil airliner crashes since 1950*, Sparkford : Patrick Stephens, 2006.

[3] Burcham, F. W., Maine, T. A., Burken, J., and Bull, J., "Using Engine Thrust for Emergency Flight Control: MD–11 and B–747 Results," Technical Memorandum NASA/TM–1998–206552, NASA, 1998.

[4] Burcham, F. W., Maine, T. A., Kaneshinge, J., and Bull, J., "Simulator evaluation of simplified propulsion–only emergency flight control system on transport aircraft," Tech. Rep. NASA/TM-1999-206578, NASA, 1999.

[5] Burcham, F. W., Burken, J., Maine, T. A., and Bull, J., "Emergency Flight Control Using Only Engine Thrust and Lateral Center-of-Gravity Offset: A First Look," Technical Memorandum NASA/TM-4789, NASA, 1997.

[6] Tucker, T., *Touchdown: the development of propulsion controlled aircraft at NASA Dryden*, Monographs in Aerospace History, No. 16, 1999.

[7] Burken, J., Burcham, J. W., Trindel, A. M., Feather, J., Goldthorpe, S., and Kahler, J., "Flight test of propulsion–based emergency control system on the MD–11 airplane with emphasis on the lateral axis," Tech. Rep. NASA/TM-4746, NASA, 1996.

[8] Smaili, M. H. and Mulder, J. A., "Flight data reconstruction and simulation of the 1992 Amsterdam Bijlmermeer airplane accident," *AIAA Modeling and Simulation Technologies Conference*, 2000.

[9] Maciejowski, J. M. and Jones, C. N., "MPC fault-tolerant control case study: flight 1862," *Proceedings of the IFAC Symposium SAFEPROCESS '03, Washington*, 2003, pp. 119-124.

[10] Hennig, A. and Balas, G. J., "MPC Supervisory Flight Controller: A Case Study to Flight EL AL 1862," *AIAA Guidance, Navigation and Control Conference and Exhibit*, 2008.

[11] Lombaerts, T. J. J., Huisman, H. O., Chu, Q. P., Mulder, J. A., and Joosten, D. A., "Flight Control Reconfiguration based on Online Physical Model Identification and Nonlinear Dynamic Inversion," *AIAA Guidance, Navigation and Control Conference and Exhibit*, No. AIAA 2008-7435, 2008.

[12] Stroosma, O., Smaili, H., Lombaerts, T., and Mulder, J. A., "Piloted Simulator Evaluation of New Fault-Tolerant Flight Control Algorithms for Reconstructed Accident Scenarios," *AIAA Modeling and Simulation Technologies Conference and Exhibit*, 2008.

[13] Shtessel, Y., Buffington, J., and Banda, S., "Tailless Aircraft Flight Control Using Multiple Time Scale Re-configurable Sliding Modes," *IEEE Transactions on Control Systems Technology*, Vol. 10, No. 2, 2002, pp. 288–296.

[14] Wells, S. R. and Hess, R. A., "Multi–input/multi–output sliding mode control for a tailless fighter aircraft," *Journal of Guidance, Control and Dynamics*, Vol. 26, 2003, No. 3, pp. 463–473.

[15] Alwi, H. and Edwards, C., "Model-Reference Sliding Mode FTC With On-line Control Allocation," *46th IEEE Conference on Decision and Control*, 2007.

[16] Alwi, H. and Edwards, C., "Fault tolerant control using sliding modes with on-line control allocation," *Automatica*, Vol. 44, No. 7, 2008, pp. 1859–1866.

[17] Alwi, H., Edwards, C., Stroosma, O., and Mulder, J. A., "Fault Tolerant Sliding Mode Control Design with Piloted Simulator Evaluation," *AIAA Journal of Guidance, Control and Dynamics*, Vol. 31, No. 5, 2008, pp. 1186–1201.

[18] Patton, R. J., "Robustness in model-based fault diagnosis: the 1997 situation," *IFAC Annual Reviews*, 1997, Vol. 21, 2008, pp. 101-121.

[19] Zhang, Y. and Jiang, J., "Bibliographical review on reconfigurable fault tolerant control systems," *Proceedings of the IFAC Symposium SAFEPROCESS '03, Washington*, 2003, pp. 265–276.

[20] van der Linden, C. A. A. M., "DASMAT: Delft University aircraft simulation model and analysis tool," Tech. Rep. LR–781, Technical University of Delft, the Netherlands, 1996.

[21] Smaili, M. H., "FLIGHTLAB 747: Benchmark for Advance Flight Control Engineering," Tech. rep., Technical University Delft, the Netherlands, 1999.

[22] Marcos, A. and Balas, G. J., "A Boeing 747–100/200 Aircraft Fault Tolerant and Diagnostic Benchmark," Tech. Rep. AEM–UoM–2003–1, Department of Aerospace and Engineering Mechanics, University of Minnesota, 2003.

[23] Marcos, A. and Balas, G. J., "A robust integrated controller/diagnosis aircraft application," *International Journal of Robust and Nonlinear Control*, Vol. 15, No. 12, 2005, pp. 531–551.

[24] Marcos, A., Ganguli, S., and Balas, G. J., "An application of H_∞ fault detection and isolation to a transport aircraft," *Control Engineering Practice*, Vol. 13, No. 1, 2005, pp. 105–119.

[25] Szaszi, I., Marcos, A., Balas, G. J., and Bokor, J., "Linear parameter-varying detection filter design for a Boeing 747-100/200 aircraft," *Journal of Guidance, Control, and Dynamics*, Vol. 28, No. 3, 2005, pp. 461–470.

[26] Zhou, K., Rachinayani, P. K., Liu, N., Ren, Z., and Aravna, J., "Fault Diagnosis and Reconfigurable Control for Flight Control Systems with Actuator Failures," *43rd IEEE Conference on Decision and Control, Bahamas*, 2004.

[27] Smaili, M. H., Breeman, J., Lombaerts, T. J. J., and Joosten, D. A., "A simulation benchmark for integrated fault tolerant flight control evaluation," *AIAA Modeling and Simulation Technologies Conference and Exhibit*, 2006.

[28] Stroosma, O., van Paassen, M. M., and Mulder, M., "Using the SIMONA Research Simulator for Human-machine Interaction Research," *AIAA Modeling and Simulation Technologies Conference*, 2003.

[29] Anon, "EL AL Flight 1862, Aircraft Accident Report 92-11," Tech. rep., Netherlands Aviation Safety Board, Hoofddorp, 1994.

[30] Shin, D., Moon, G., and Kim, Y., "Design of reconfigurable flight control system using adaptive sliding mode control: actuator fault," *Proceedings of the Institution of Mechanical Engineers, Part G (Journal of Aerospace Engineering)*, Vol. 219, No. 4, 2005, pp. 321–328.

[31] Härkegård, O. and Glad, S. T., "Resolving actuator redundancy - optimal control vs. control allocation," *Automatica*, Vol. 41, No. 1, 2005, pp. 137–144.

[32] Härkegård, O., *Backstepping and Control Allocation with Applications to Flight Control*, Ph.D. thesis, Division of Automatic Control, Department of Electrical Engineering Linköping University, Sweden, 2003.

[33] Beck, R. E., *Application of Control Allocation Methods to Linear Systems with Four or More Objectives*, Ph.D. thesis, Virginia Polytechnic Institute and State University, Blacksburg, Virginia, 2002.

[34] Horn, R. and Johnson, C., *Matrix Analysis*, Cambridge University Press, 1990, pp. 421.
[35] Penrose, R., "A generalized inverse for matrices," *Proceedings of the Cambridge Philosophical Society*, Vol. 51, 1955, pp. 406–413.
[36] Enns, D., "Control Allocation Approaches," *AIAA Guidance, Navigation and Control Conference and Exhibit*, 1998, pp. 98–108.
[37] Durham, W. C., "Constrained control allocation," *Journal of Guidance, Control, and Dynamics,*, Vol. 16, No. 4, 1993, pp. 717–25.
[38] Landau, I., "Survey of model-reference adaptive techniques," *Automatica*, Vol. 10, No. 4, 1974, pp. 353–379.
[39] Landau, I. and Courtoil, B., "Design of multivariable adaptive model-following control systems," *Automatica*, Vol. 10, No. 5, 1974, pp. 483–494.
[40] Monopoli, R. V. and Subbarao, V. N., "Design of a multivariable model following adaptive control system," *Proceedings of the 20th IEEE Conference on Decision and Control including the Symposium on Adaptive Processes*, 1981, pp. 992–998.
[41] Broussard, J. R. and O'Brien, M. J., "Feedforward control to track the output of a forced model," *IEEE Transactions on Automatic Control*, Vol. AC-25, No. 4, 1980, pp. 851–853.
[42] Zinober, A. S. I., El-Ghezawi, O. M. E., and Billings, S. A., "Multivariable variable-structure adaptive model-following control systems," *Proceedings of the IEE, Part D*, Vol. 129, 1982, pp. 6–12.
[43] Utkin, V. I., *Sliding Modes in Control Optimization*, Springer-Verlag, Berlin, 1992, ch. 3.
[44] Edwards, C. and Spurgeon, S. K., *Sliding Mode Control: Theory and Applications*, Taylor & Francis, 1998, ch. 3–4.
[45] Alwi, H. and Edwards, C., "Sliding mode FTC with on–line control allocation," *45th IEEE Conference on Decision and Control*, 2006.
[46] Stewart, G. W., "On Scaled Projections and Pseudoinverses," *Linear Algebra and Its Applications*, Vol. 112, 1989, pp. 189–193.
[47] Khalil, H., *Nonlinear Systems*, Prentice Hall, Englewood Cliffs NJ., 1992, ch. 5.
[48] Liu, G. P. and Patton, R. J., *Eigenstructure Assignment for Control System Design*, John Wiley & Sons, 1998, ch. 2.
[49] Hanke, C. and Nordwall, D., "The simulation of a Jumbo Jet Transport Aircraft. Volume II: Modelling Data," Tech. Rep. CR-114494/D6-30643-VOL2, NASA and The Boeing Company, 1970.
[50] Hanke, C., "The simulation of a Large Jet Transport Aircraft. Volume I: Mathematical Model," Tech. Rep. CR-1756, NASA and the Boeing company, 1971.
[51] Bošković, J. D. and Mehra, R. K., *Fault Diagnosis and Fault Tolerance for Mechatronic Systems: Recent Advances*, chap. Failure Detection, Identification and Reconfiguration in Flight Control, Springer-Verlag, 2002.
[52] Ganguli, S., Marcos, A., and Balas, G. J., "Reconfigurable LPV control design for Boeing 747-100/200 longitudinal axis," *American Control Conference*, 2002, pp. 3612–3617.